CORONAVIRUS

A persistent neutrophil-associated immune signature characterizes post–COVID-19 pulmonary sequelae

Peter M. George[1,2], Anna Reed[1,2], Sujal R. Desai[1,2], Anand Devaraj[1,2], Tasnim Shahridan Faiez[3], Sarah Laverty[4], Amama Kanwal[5], Camille Esneau[5], Michael K.C. Liu[4], Faisal Kamal[6], William D.-C. Man[1,2,7], Sundeep Kaul[1], Suveer Singh[1], Georgia Lamb[1], Fatima K. Faizi[3], Michael Schuliga[5], Jane Read[5], Thomas Burgoyne[1,8], Andreia L. Pinto[1], Jake Micallef[9], Emilie Bauwens[9], Julie Candiracci[9], Mhammed Bougoussa[9], Marielle Herzog[9], Lavanya Raman[2], Blerina Ahmetaj-Shala[2], Stuart Turville[10], Anupriya Aggarwal[10], Hugo A. Farne[2,11], Alessia Dalla Pria[4,12], Andrew D. Aswani[13,14], Francesca Patella[15], Weronika E. Borek[15], Jane A. Mitchell[2], Nathan W. Bartlett[5], Arran Dokal[15], Xiao-Ning Xu[4], Peter Kelleher[1,12,16,17], Anand Shah[1,18]*†, Aran Singanayagam[3]*†

Interstitial lung disease and associated fibrosis occur in a proportion of individuals who have recovered from severe acute respiratory syndrome coronavirus 2 (SARS-CoV-2) infection through unknown mechanisms. We studied individuals with severe coronavirus disease 2019 (COVID-19) after recovery from acute illness. Individuals with evidence of interstitial lung changes at 3 to 6 months after recovery had an up-regulated neutrophil-associated immune signature including increased chemokines, proteases, and markers of neutrophil extracellular traps that were detectable in the blood. Similar pathways were enriched in the upper airway with a concomitant increase in antiviral type I interferon signaling. Interaction analysis of the peripheral phosphoproteome identified enriched kinases critical for neutrophil inflammatory pathways. Evaluation of these individuals at 12 months after recovery indicated that a subset of the individuals had not yet achieved full normalization of radiological and functional changes. These data provide insight into mechanisms driving development of pulmonary sequelae during and after COVID-19 and provide a rational basis for development of targeted approaches to prevent long-term complications.

INTRODUCTION

Clinical presentation after infection with severe acute respiratory syndrome coronavirus 2 (SARS-CoV-2) is broad, ranging from a mild self-limiting illness to severe respiratory failure requiring intensive support (1). Numerous studies have assessed the early acute phases of coronavirus disease 2019 (COVID-19), but there has been relatively less focus on the longer-term sequelae induced by this infectious disease. Most of the affected individuals make a full clinical recovery; however, a substantial proportion experience long-term health consequences, and a diverse range of symptoms have been described as part of the post–COVID-19 syndrome (2–4). Persistent radiological abnormalities associated with pulmonary function impairment occur in some infected individuals (5–8), but the pathogenic mechanisms underlying this downstream consequence are poorly characterized.

Clinical studies reveal that patients with severe COVID-19–related acute respiratory distress syndrome are at greatest risk of pulmonary complications (9, 10). However, the reasons why some individuals make a full clinical, physiological, and radiological recovery while others follow a more perilous trajectory, with persistent interstitial lung changes and associated pulmonary function impairment, are poorly understood. Acute severe COVID-19 is characterized by hyperinflammation detectable both systemically and within the airways (11–13), and there is growing evidence to indicate that myeloid cells are major contributors of immunopathology (13–16). Whether post–COVID-19 lung pathology is driven by persistence of this initial heightened inflammatory response or activation of alternative pathways that develop subsequent to recovery from the acute illness is unknown. Recent immunoprofiling studies have compared individuals with post–COVID-19

[1]Royal Brompton and Harefield Clinical Group, Guy's and St. Thomas' NHS Foundation Trust, London SW3 6NR, UK. [2]National Heart and Lung Institute, Imperial College London, London SW3 6LY, UK. [3]Centre for Molecular Bacteriology and Infection, Department of Infectious Disease, Imperial College London, London SW7 2DD, UK. [4]Section of Virology, Department of Infectious Disease, Imperial College London, London W2 1PG, UK. [5]Faculty of Health, Medicine and Wellbeing, Hunter Medical Research Institute, University of Newcastle, Callaghan, NSW 2308, Australia. [6]Royal Berkshire Hospital, Reading RG1 5AN, UK. [7]Faculty of Life Sciences and Medicine, King's College London, London WC2R 2LS, UK. [8]UCL Institute of Ophthalmology, University College London, London EC1V 9EL, UK. [9]Belgian Volition SRL, 22 rue Phocas Lejeune, Parc Scientifique Créalys, Isnes 5032, Belgium. [10]The Kirby Institute, University of New South Wales, Sydney, NSW 2052, Australia. [11]Chest and Allergy Department, St Mary's Hospital, Imperial College NHS Trust, London W2 1NY, UK. [12]Department of HIV and Genitourinary Medicine, Chelsea and Westminster NHS Foundation Trust, London SW10 9NH, UK. [13]Department of Intensive Care Medicine, Guy's and St Thomas' NHS Foundation Trust, London SE1 7EH, UK. [14]Santersus AG, Buckhauserstrasse 34, Zurich 8048, Switzerland. [15]Kinomica Ltd, Biohub, Alderley Park, Alderley Edge, Macclesfield, Cheshire SK10 4TG, UK. [16]Immunology of Infection Section, Department of Infectious Disease, Imperial College London, London W2 1PG, UK. [17]Department of Infection and Immunity Sciences, North West London Pathology NHS Trust, London W2 1NY, UK. [18]MRC Centre of Global Infectious Disease Analysis, Department of Infectious Disease Epidemiology, School of Public Health, Imperial College London, London W2 1PG, UK.
*Corresponding author. Email: s.anand@imperial.ac.uk (A. Shah); a.singanayagam@imperial.ac.uk (A. Singanayagam)
†These authors contributed equally to this work.

lung parenchymal abnormalities to healthy controls and identified increases in airway CD8^{+} and CD4^{+} T lymphocytes, with gene expression associated with myeloid cell inflammation (17, 18). These studies provide information about the immunological landscape after recovery from acute SARS-CoV-2 but lack an appropriate control group, namely, individuals with resolution of lung changes after COVID-19 and so do not provide insight to distinguish the critical pathways dictating susceptibility to, or protection against, development of persistent interstitial lung changes.

A diverse range of etiological factors and associated mechanisms are known to drive pathogenesis of other interstitial lung diseases (19). The COVID-19 pandemic offers a unique opportunity to study mechanisms of fibrogenesis in individuals with a defined common etiology. Here, we used longitudinal systemic and upper airway sampling in a cohort of individuals hospitalized with severe COVID-19 to compare those who have persistent interstitial lung changes to those with full radiographic resolution and to elucidate the immune mechanisms that drive this downstream complication. Using a multiomic approach to gain broad unbiased insight, we identified that the development of post–COVID-19 interstitial lung changes is associated with a proinflammatory, neutrophil-associated immune signature detectable in the plasma and upper airways with a concomitant enriched antiviral immune signature. Our findings provide fundamental insights into mechanisms driving pulmonary sequelae of COVID-19 and provide a rational basis for development of targeted therapeutic approaches to prevent longer-term complications.

RESULTS

Severe COVID-19 is associated with an up-regulated plasma immune signature after recovery from acute disease

To investigate the downstream immunological and clinical consequences after acute COVID-19, we studied 46 individuals with severe COVID-19. All participants had clinical phenotyping, cross-sectional lung imaging, respiratory function testing, and blood and nasal sampling at 3 to 6 months (mean, 129 days) after discharge from hospital (visit 1). We additionally evaluated 18 individuals with mild (nonhospitalized) COVID-19 and 17 healthy uninfected control individuals. Acute COVID-19 is characterized by mucosal and central hyperinflammation, a feature accentuated in individuals with more severe disease (11, 12, 20), but whether immune activation persists after recovery from the acute illness is less well characterized. We initially examined the peripheral plasma proteome using the Olink proteomics platform to measure 184 unique proteins (table S1) and compared the immune signatures at 3 to 6 months after discharge between those with severe COVID-19 and those with mild COVID-19 or healthy uninfected controls (Fig. 1A). The proteins measured were highly enriched for those involved in inflammation and immune processes. Principal component analysis of plasma proteomes revealed differences between those with severe and mild COVID-19 with separation of groups most evident along principal component 1 (PC1) (Fig. 1B).

To examine the effects of COVID-19 severity on the plasma proteome at 3 to 6 months, we performed differential expression analysis. This identified 63 proteins with significantly altered concentrations [5% false discovery rate (FDR)] with the majority (n = 59) up-regulated and only four proteins down-regulated

(Fig. 1, C and D). The proteins that were most increased between patients with severe COVID-19 and patients with mild COVID-19 in terms of fold change were C-X-C motif chemokine 5 (CXCL5), hexamethylene bisacetamide-inducible protein, oncostatin M, and eukaryotic translation initiation factor 4E–binding protein 1 (Fig. 1C). The down-regulated proteins were corneodesmosin (CDSN), tryptase alpha/beta 1 (TPSAB1), C-C motif chemokine ligand 11 (CCL11), and peroxiredoxin-1 (PRDX1). Representative plots showing distributions of up-regulated postrecovery plasma proteins in those with severe COVID-19, those with mild COVID-19, and healthy controls are shown in Fig. 1E. Pathway analysis of these 59 up-regulated proteins using String-DB highlighted enrichment of the following gene ontology biological processes: "immune system process," "immune response," and "cytokine-mediated signaling pathway" (Fig. 1F). Collectively, these data indicated that severe COVID-19 is associated with a persistent proinflammatory immune signature detectable in plasma at 3 to 6 months after recovery from the acute illness.

Radiographic and lung function abnormalities occur in a subset of individuals after recovery from severe COVID-19 illness

Of the 46 individuals with severe COVID-19, n = 26 (56.2%) had interstitial lung changes on computed tomography (CT) imaging at 3 to 6 months after discharge with the remaining participants (n = 20) showing no interstitial changes, indicating full resolution of parenchymal changes (fig. S1A). Demographic and clinical characteristics of this cohort are shown in table S2. Persistent interstitial change on CT at 3 to 6 months after acute illness was associated with reduced pulmonary lung function as measured by % predicted forced vital capacity (FVC) and transfer factor for carbon monoxide (TLCO) (fig. S1, B and C) and increased symptom scores as measured by St. Georges Respiratory Questionnaire (fig. S1D).

Post–COVID-19 interstitial lung changes are characterized by an augmented proinflammatory neutrophil-associated plasma immune signature

We next compared plasma proteomic profiles (again using the Olink platform) at 3 to 6 months after discharge between individuals with post–COVID-19 interstitial lung changes versus those with radiographic resolution (Fig. 2A) to gain insight into the immune pathways/mediators that might mechanistically drive this complication. Principal component analysis of plasma proteomes revealed differences between those with post–COVID-19 interstitial changes and those with resolution, most evident along PC1 (Fig. 2B). Differential protein abundance analysis identified 30 proteins with significantly altered concentrations (5% FDR) with the majority (n = 26) up-regulated and four proteins down-regulated (Fig. 2, C and D). The proteins that were most increased between individuals with interstitial lung changes and those with resolution (in terms of fold change) were the proinflammatory cytokines interleukin-17C (IL-17C), extracellular newly identified receptor for advanced glycation end-products binding protein (EN-RAGE), CCL20, CCL25, and tumor necrosis factor (TNF) (Fig. 2D). Down-regulated proteins were the same as those attenuated at 3 to 6 months in all severe versus mild COVID-19 individuals (CDSN, TPSAB1, CCL11, and PRDX1; Fig. 1D). Representative violin plots showing distributions of selected up-regulated plasma proteins in those with interstitial lung changes and those with
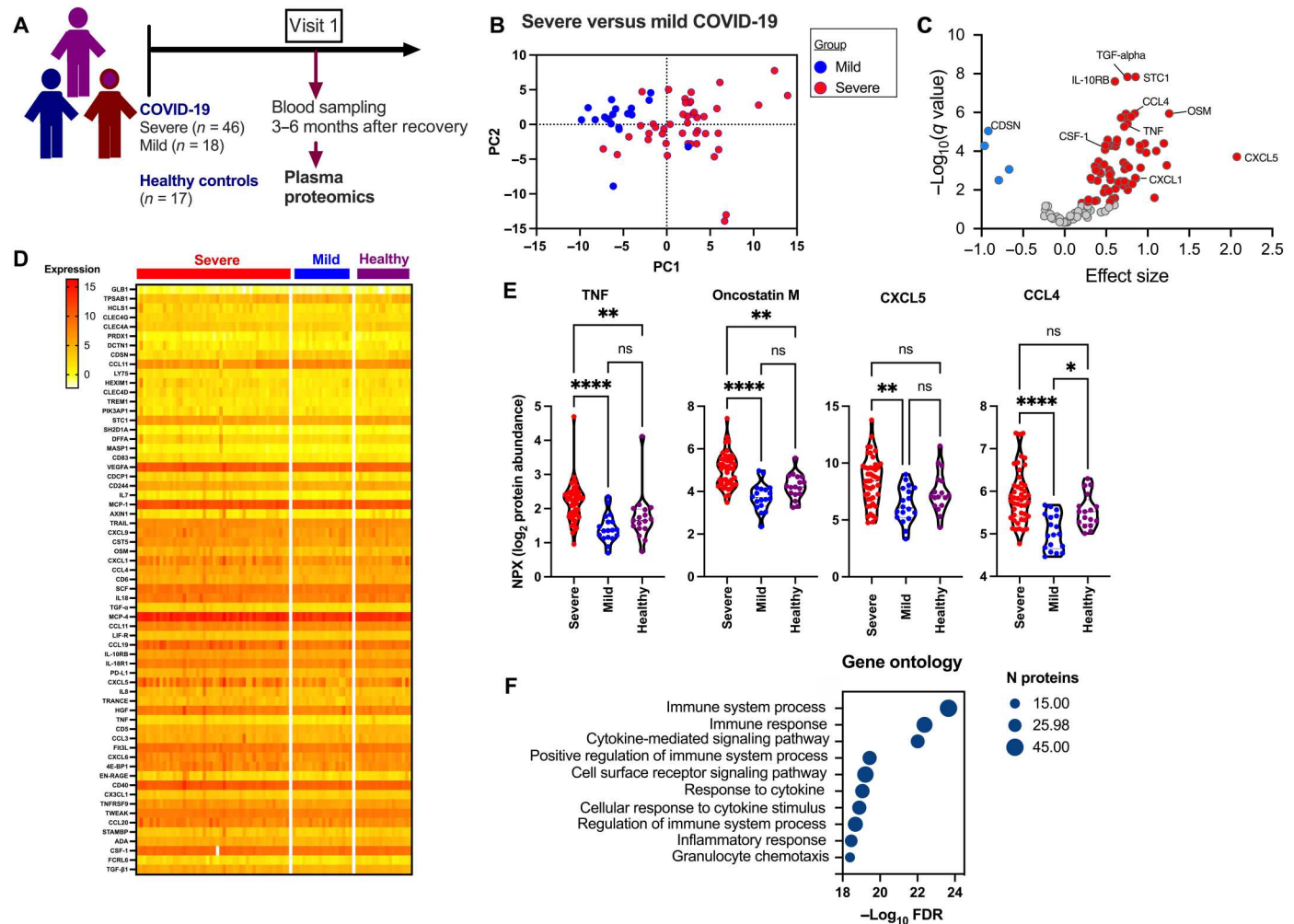
Fig. 1. Up-regulated systemic immune signature is observed at 3 to 6 months after severe COVID-19. (**A**) Timeline of study. (**B**) Principal component analysis is shown. Each point represents a sample. Coloring indicates COVID-19 severity. (**C**) Proteins that were up-regulated (red) or down-regulated (blue) in patients with severe COVID-19 versus those with mild COVID-19 are shown for samples collected at 3 to 6 months after recovery from acute illness. The linear gradient indicates the effect size. A positive effect size (right side of the graph) indicates that an increase in protein concentrations is associated with severe COVID-19 cases, and a negative gradient (left side of graph) indicates the opposite. P values are from linear mixed models after Benjamini-Hochberg adjustment; significance threshold = 5% FDR; gray = nonsignificant. (**D**) Heatmap showing protein concentrations. Each column represents a sample ($n = 46$ severe COVID-19 samples, $n = 18$ mild COVID-19 samples, and $n = 17$ healthy controls). Each row represents a protein. Differentially expressed proteins between severe COVID-19 versus mild COVID-19 groups are shown. (**E**) Violin plots show the distribution of selected plasma protein concentrations [normalized protein expression (NPX)] at 3 to 6 months after severe or mild COVID-19 and in healthy uninfected controls. Boxplots indicate median, interquartile range (IQR), minimum, and maximum. Data in (E) were analyzed using Kruskal-Wallis test with Dunn's posttest. ns, not significant; *$P < 0.05$, **$P < 0.01$, and ****$P < 0.0001$. (**F**) Gene ontology biological processes enrichment analysis is shown for the differentially expressed proteins.

resolution are shown in Fig. 2E. Enrichment analysis of immune pathways of the 26 up-regulated proteins using String-DB highlighted gene ontology biological processes including "neutrophil chemotaxis," "humoral immune response," and "defense response" (Fig. 2F). Given that individuals with post–COVID-19 interstitial changes differed from those with resolution with regard to several factors (such as age, body mass index, and initial disease severity; see table S2), which may themselves be associated with greater initial inflammatory responses (and thus a persistence of inflammation), we conducted a multivariable analysis to determine whether up-regulated proteins remained independently associated with the presence of interstitial lung changes after adjustment for confounding variables ($P < 0.1$ on univariate analysis; see table S2). This

revealed that the neutrophil-associated cytokine IL-17C was the only plasma protein independently associated with the development of interstitial changes [odds ratio (OR) 3.72; 95% confidence interval, 1.20 to 16.84; $P = 0.0403$], further supporting a role for a neutrophil-related immune signature in driving this complication.

To gain greater insight into the mediators/pathways involved in development of post–COVID-19 interstitial lung changes, we additionally investigated for correlations between measured immune proteins and severity of radiological changes or lung function impairment. In keeping with our finding that "neutrophil chemotaxis" was the most enriched immune pathway associated with interstitial lung changes (Fig. 2G), the neutrophil chemokines CXCL1 and CXCL8 negatively correlated with % FVC. CXCL8 and the
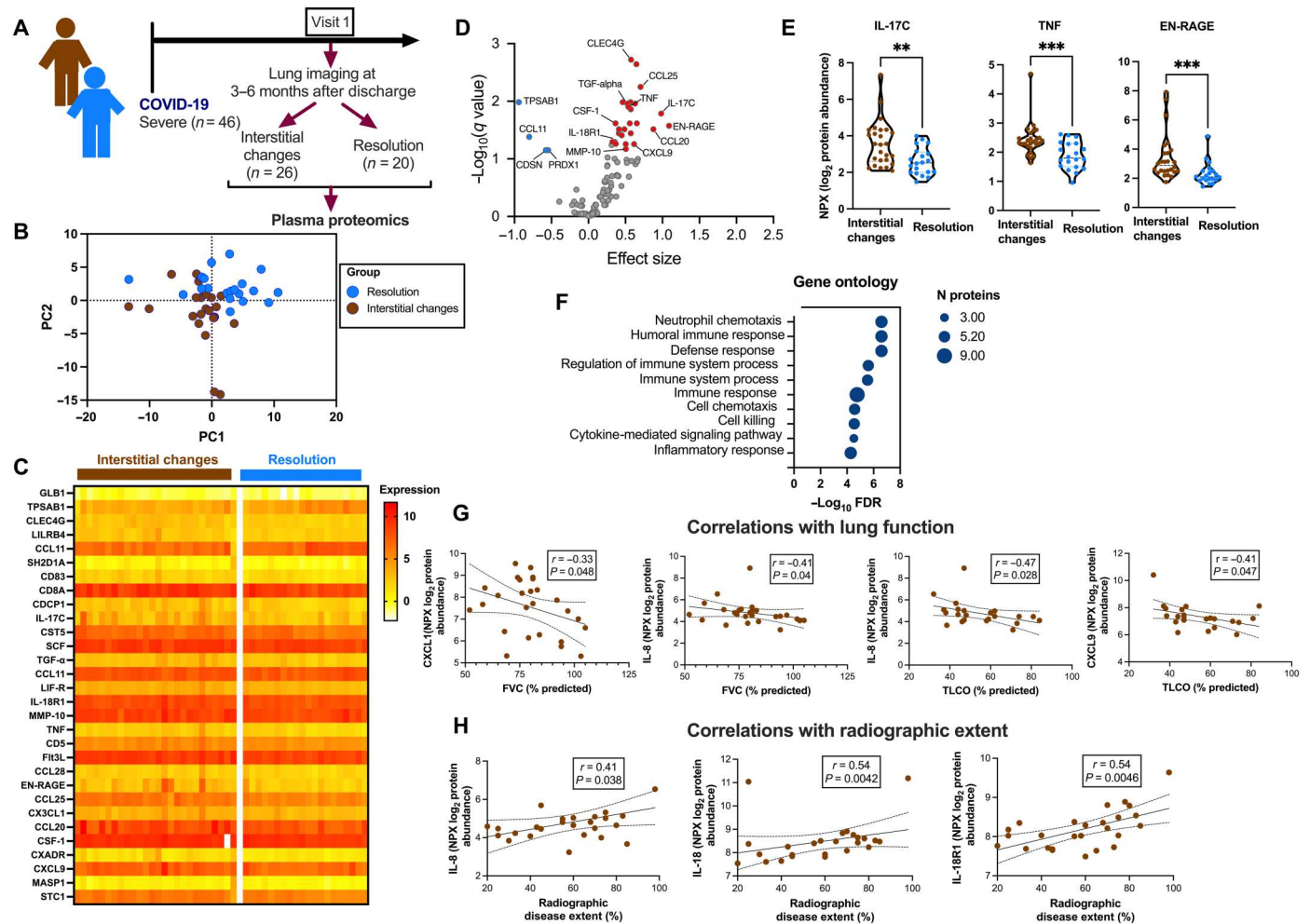
George *et al.*, *Sci. Transl. Med.* 14, eabo5795 (2022)   16 November 2022

3 of 16

Fig. 2. An up-regulated systemic proinflammatory neutrophil-associated immune signature characterizes post–COVID-19 interstitial lung changes. (**A**) Timeline of study. (**B**) Principal component analysis is shown, where each point represents a sample. Coloring indicates the presence or absence of interstitial lung changes. (**C**) The heatmap shows protein concentrations. Each column represents a sample (n = 26 individuals with interstitial lung changes and n = 20 with full resolution of lung changes). Each row represents a protein. Differentially expressed proteins between severe COVID-19 versus mild COVID-19 groups are shown. (**D**) Proteins up-regulated (red) or down-regulated (blue) in individuals with interstitial lung changes after recovery are shown. The linear gradient indicates the effect size. A positive effect size (right side of graph) indicates that an increase in protein concentration is associated with the presence of interstitial lung changes, and a negative gradient (left side of graph) indicates the opposite. P values are from linear mixed models after Benjamini-Hochberg adjustment; significance threshold = 5% FDR; gray = nonsignificant. (**E**) Violin plots showing distribution of selected plasma protein concentrations at 3 to 6 months in individuals with interstitial lung changes versus those without. Boxplots indicate median, IQR, minimum, and maximum. Data in (E) were analyzed using Mann-Whitney U test. **P < 0.01 and ***P < 0.001. (**F**) Gene ontology biological processes enrichment analysis is shown for the differentially expressed proteins. (**G**) Correlation between plasma proteins and lung function measurements, including % predicted of forced vital capacity (FVC) and transfer factor for carbon monoxide (TLCO), is shown. (**H**) Correlation between plasma proteins and extent of radiographic changes on CT scanning is shown. Correlations were determined by Spearman's rank correlation test.

interferon (IFN)−inducible lymphocyte chemokine CXCL9 also negatively correlated with % TLCO. For radiological disease extent, positive correlations were observed for CXCL8, the inflammasome-associated proinflammatory cytokine IL-18, and its receptor IL-18R1 (Fig. 2H). Collectively, these data reveal that post–COVID-19 interstitial lung changes are associated with a persistent plasma neutrophil-associated proinflammatory immune signature.

Post–COVID-19 interstitial lung changes are associated with an up-regulated proinflammatory and antiviral immune signature in the upper airways

The nose is a major entry site for SARS-CoV-2 and therefore represents the primary mucosal site of initial host immune responses (21, 22). Given our findings that post–COVID-19 interstitial lung changes were characterized by an up-regulated systemic proinflammatory immune signature, we next sought to determine whether similar changes occurred within the upper airways by evaluating nasal brushing samples taken at the same time point (3 to 6 months after hospital discharge). Of the 46 participants with severe COVID-19 included in the study, 26 individuals (n = 16

George *et al.*, *Sci. Transl. Med.* **14**, eabo5795 (2022)   16 November 2022

4 of 16

with interstitial lung changes and $n = 10$ resolved) had samples with sufficient RNA concentration and of high enough quality to perform transcriptomic analysis (Fig. 3A), for which we used the Nanostring NCounter multiplex platform that profiles more than 850 immune response genes (table S3).

Principal component analysis of nasal transcriptomes at 3 to 6 months after discharge revealed differences between those with post–COVID-19 interstitial changes versus those with resolution, most evident along PC1 (Fig. 3B), although differences were less marked than for plasma (Fig. 2B), and there was considerable overlap in the spatial location of individuals with interstitial changes and those with resolution. Differential gene expression

analysis identified 53 genes (5% FDR) up-regulated in individuals with interstitial changes versus those with resolution. The genes most substantially up-regulated were predominantly broadly related to antiviral defense (*GBP5*, *IFIT2*, and *OASL*) or neutrophilic inflammation/inflammasome pathways (*CXCL8*, *CXCR2*, *IL1R2*, and *NLRP3*) (Fig. 3, C and D). Representative violin plots showing distributions of selected up-regulated immune genes in subjects with interstitial lung changes and those with full resolution are shown in Fig. 3E. This global activation of antiviral and proinflammatory signatures was further supported by enrichment analysis of immune pathways, which indicated gene ontology biological processes related to the "cytokine-mediated signaling pathway" and
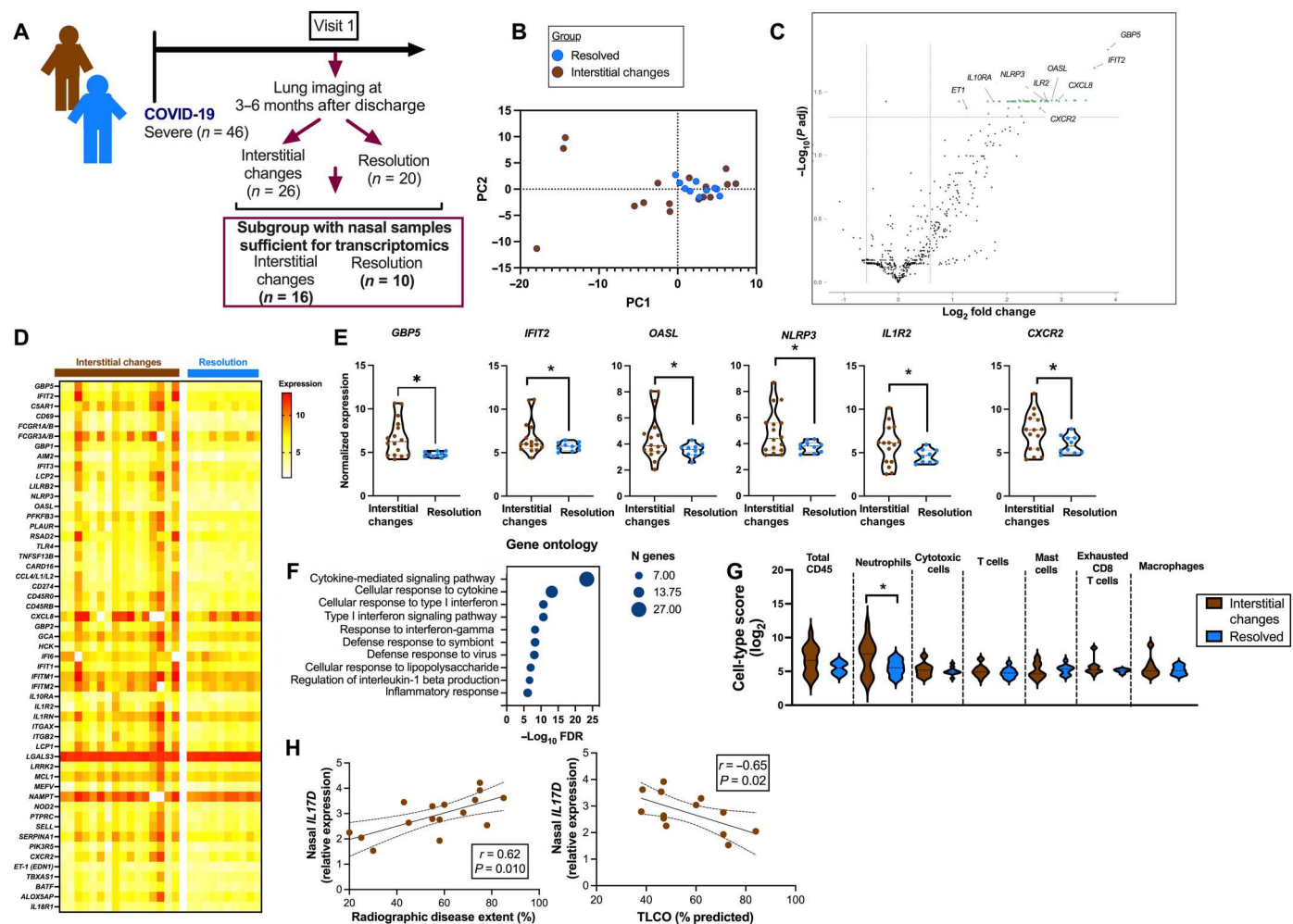

Fig. 3. An up-regulated nasal proinflammatory and antiviral immune signature characterizes post–COVID-19 interstitial lung changes. (**A**) Study timeline. (**B**) Principal component analysis is shown, where each point represents a sample. Coloring indicates the presence or absence of interstitial lung changes. (**C**) Genes up-regulated (right) and down-regulated (left) in individuals with interstitial lung changes after recovery are shown. Linear gradient indicates the effect size. A positive effect size (right side of the graph) indicates that an increase in gene expression is associated with the presence of interstitial lung changes, and a negative gradient (left side of the graph) indicates the opposite. *P* values are from linear mixed models after Benjamini-Hochberg adjustment; significance threshold = 5% FDR. (**D**) The heatmap shows gene expression. Each column represents a sample ($n = 16$ individuals with interstitial lung changes and $n = 10$ with full resolution of lung changes). Each row represents a gene. Differentially expressed genes between severe COVID-19 versus mild COVID-19 groups are shown. (**E**) Violin plots show the distribution of selected genes at 3 to 6 months in individuals with interstitial lung changes versus those without. Boxplots indicate median, IQR, minimum, and maximum. (**F**) Gene ontology biological processes enrichment analysis are shown for the differentially expressed genes. (**G**) Cellular deconvolution analysis of transcriptomic data is shown. Boxplots indicate median, minimum, and maximum. (**H**) The correlations between *IL17D* expression and extent of radiographic changes by CT scan (left) and lung % predicted TLCO (right) are shown. Correlation analysis in (H) was conducted using Spearman's rank correlation test. Statistical analysis in (E) and (G) was conducted using Mann-Whitney *U* test. *$P < 0.05$.

the "cellular response to type I interferon" (Fig. 3F), and by cellular deconvolution analysis, which indicated an enrichment of neutrophils in individuals with post–COVID-19 interstitial lung changes (Fig. 3G). Nasal *IL17D* expression correlated positively with radiographic disease extent and negatively with % TLCO (Fig. 3H). These data fit with existing paradigms, suggesting that increased SARS-CoV-2 viral load in the upper respiratory tract associated with severe disease drives a type I IFN signature that contributes to subsequent hyperinflammation and disease severity (*23*). These findings also suggest that these differences persist in individuals who have post–COVID-19 interstitial lung changes.

Post–COVID-19 interstitial lung changes are associated with increased systemic neutrophils, protease concentrations, and markers of NET formation

Having identified an up-regulated neutrophil-associated immune signature in individuals with post–COVID-19 interstitial lung changes, we hypothesized that increased neutrophils in these individuals may drive fibrogenesis through formation of neutrophil extracellular traps (NETs) and consequent release of extracellular matrix (ECM)–degrading neutrophil proteases. We therefore evaluated total neutrophil counts, neutrophil protease concentrations, and markers of NET formation in plasma taken from individuals with interstitial lung changes compared to those with resolution (Fig. 4A). Total neutrophil numbers were increased in individuals with post–COVID-19 interstitial changes compared to those with radiographic resolution (Fig. 4B). A similar increase was observed for plasma concentrations of the neutrophil protease

myeloperoxidase (Fig. 4C), which also correlated positively with radiological disease extent and negatively with lung function impairment (% TLCO) (Fig. 4D). There were no differences in plasma neutrophil elastase or extracellular DNA concentrations between the two groups (figs. S2 and S3). NETosis involves hypercitrullination of nucleosomal histone proteins, including H3, which can be quantified in plasma as a remnant of NET formation. Concentrations of H3R8 citrullinated nucleosomes were increased in individuals with post–COVID-19 interstitial changes compared to those with radiographic resolution (Fig. 4E). However, this effect was not observed when comparing the total amount of circulating intact nucleosomes as measured by the canonical H3.1 nucleosomes assay (Fig. 4F).

Post–COVID-19 interstitial lung changes are associated with up-regulated proinflammatory immune phosphoproteome signatures

To better understand the mechanisms underlying perturbation of inflammatory signaling in individuals with post–COVID-19 interstitial changes, we performed phosphoproteomic analysis of peripheral blood mononuclear cells (PBMCs) taken from a subgroup of individuals at the same 3- to 6-month time point (Fig. 5A). Principal component analysis of the phosphoproteomic results revealed that there were distinct differences between PBMCs isolated from individuals exhibiting interstitial changes compared to those with resolution (Fig. 5B). Despite this clustering, there was heterogeneity observed across PBMC samples derived from individuals with interstitial changes. Differential expression analysis of 5934
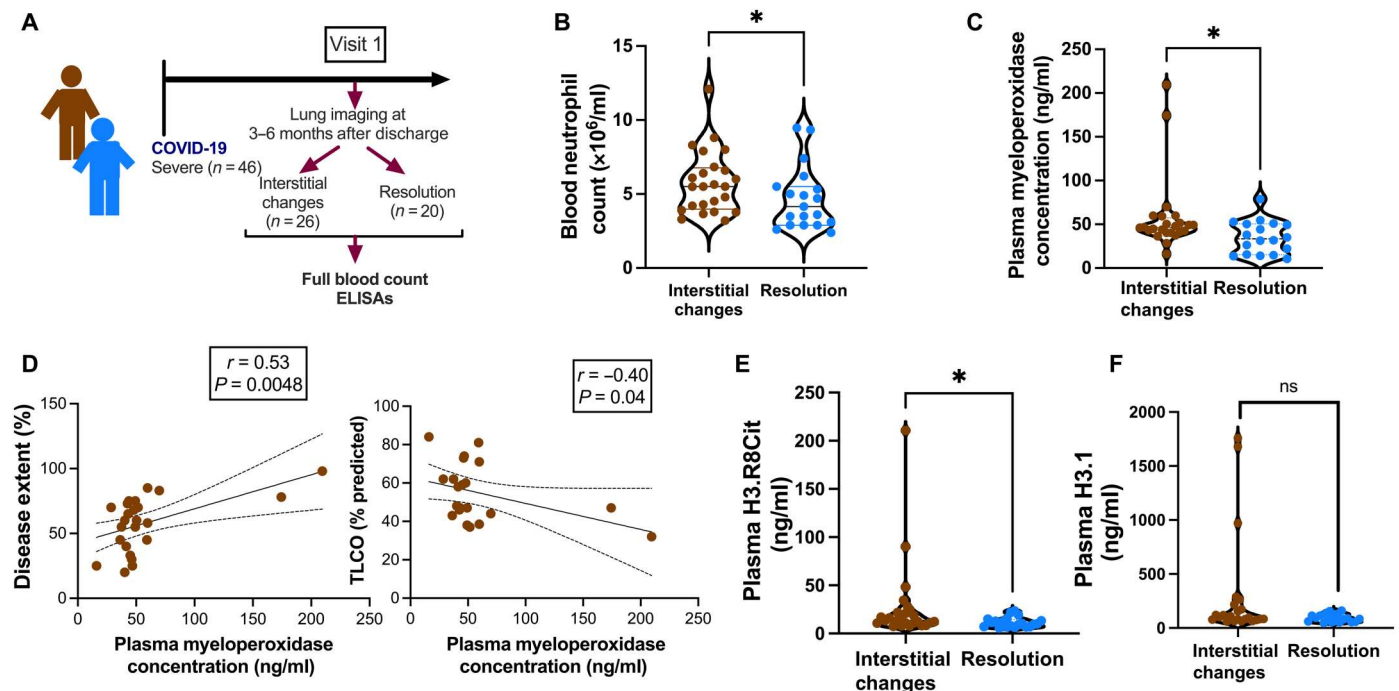
Fig. 4. Increased systemic neutrophils, neutrophil protease, and NET concentrations are associated with post–COVID-19 interstitial lung changes. (**A**) Study timeline. (**B**) Total neutrophil counts were measured in blood taken at 3 to 6 months after discharge from severe COVID-19. (**C**) Plasma myeloperoxidase concentrations were quantified by enzyme-linked immunosorbent assay (ELISA). (**D**) The correlations between plasma myeloperoxidase concentrations and extent of radiographic changes by CT scan (left) and % predicted TLCO (right) are shown. Plasma concentrations of (**E**) H3.R8 citrullinated nucleosomes and (**F**) total intact nucleosomes were measured by H3.1 ELISA. In (B), (C), (E), and (F), boxplots indicate median, minimum, and maximum; data were analyzed by Mann-Whitney U test. In (D), data were analyzed by Spearman's rank correlation test. *P < 0.05.
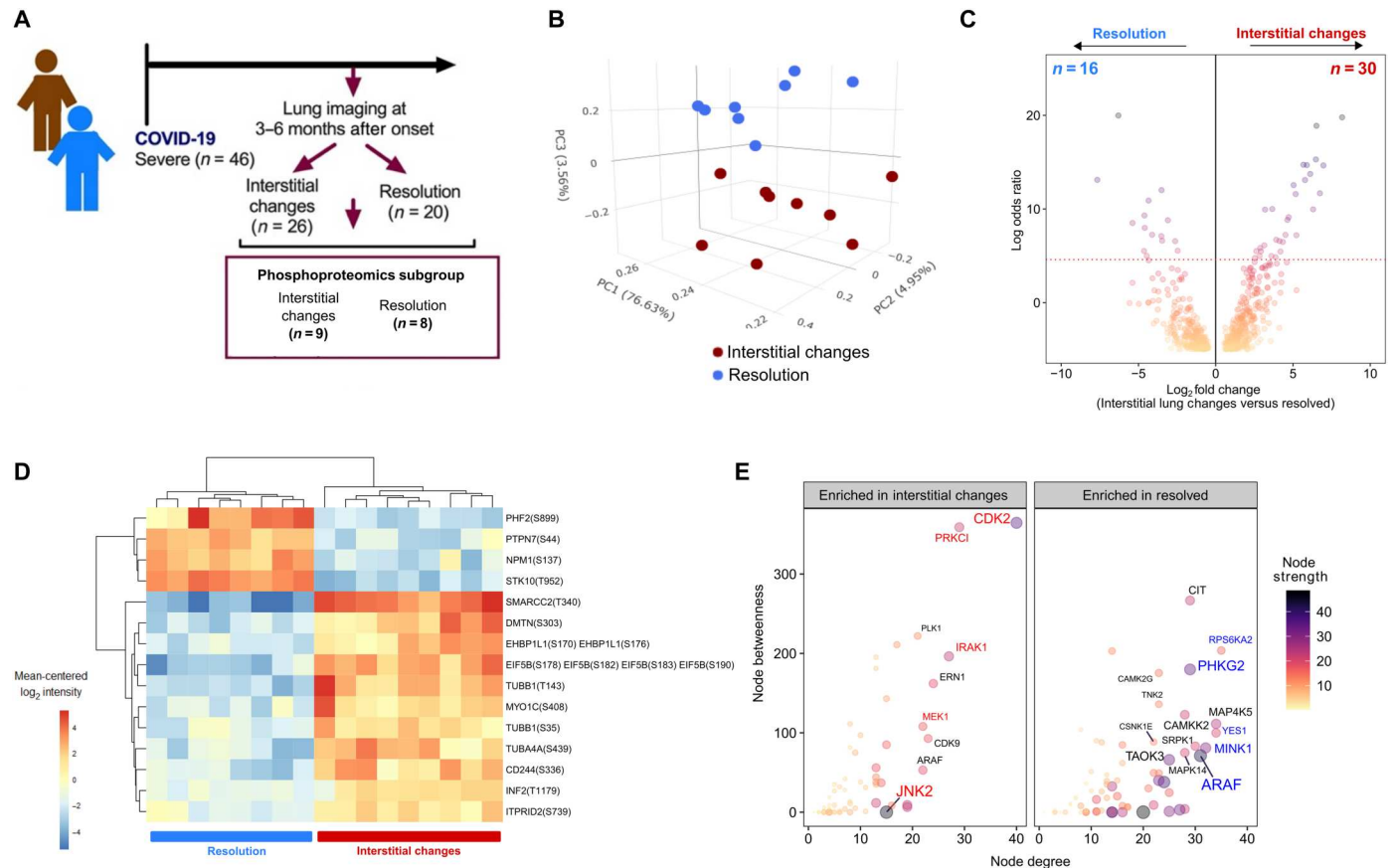
Fig. 5. Protein phosphorylation and kinase activities associated with immune cell responses are enriched in PBMCs from patients with COVID-19 interstitial lung changes. (**A**) Study timeline. (**B**) Principal component analysis is shown, where each point represents a sample and the proportion of the total variance explained by each principal component is shown in parentheses of the plot axes. Coloring indicates the presence or absence of interstitial lung changes. (**C**) The volcano plot shows phosphopeptides differentially expressed in the PBMCs of patients with COVID-19 interstitial lung changes versus those that have resolved. Points represent individual phosphopeptides colored according to the log OR of being differentially expressed. The dotted red line indicates an arbitrary threshold of a 99% probability of being differentially expressed (a log OR > 4.60). (**D**) The heatmap shows phosphorylation sites that are differentially regulated (FDR < 0.05) between patients with interstitial lung changes versus resolved. Each column represents a sample (n = 9 individuals with interstitial lung changes and n = 8 with full resolution of lung changes). Each row represents a phosphopeptide containing one to four phosphorylated sites. (**E**) Kinase network analysis is shown using characteristics computed from the KSEA network results. Points (kinases) are colored according to their node strength (the sum of weights of links connected to the kinase; interstitial lung changes versus resolved). Node betweenness (y axis) represents the degree to which kinases stand between each other (betweenness centrality indicates the control a kinase has over the network); node degree (x axis) represents the number of connections a kinase has to other kinases. The left panel represents kinases that are more important to maintaining the signaling activity in interstitial lung changes samples, and the right panel represents kinases that are integral to the samples derived from patients with resolved changes.

phosphopeptides identified 30 phosphopeptides significantly enriched (log OR > 4.6 to 99% probability of being differentially expressed) in individuals with interstitial changes compared to those with complete resolution and 16 phosphopeptides in the resolved group (Fig. 5C). An examination of sites that were differentially regulated between the groups with consistent intragroup phosphorylation identified a group of 15 phosphorylation markers (Fig. 5D). Four phosphorylation sites [plant homeodomain PHD finger protein 2 (PHF2)^{S899}, protein tyrosine phosphatase nonreceptor type 7 (PTPN7)^{S44}, nucleophosmin (NPM1)^{S137}, and serine/threonine-protein kinase 10 (STK10)^{T952}] exhibited increased phosphorylation in all resolved individuals compared to those with interstitial changes, one of which, STK10, is involved in regulating lymphocyte migration (*24*). The 11 phosphorylation sites that were increased in all individuals with interstitial changes were located on proteins implicated in phagosome action [tubulin beta-1 chain (TBB1)^{S35},

TBB1^{T143}, and tubulin alpha-4A chain (TUBA4A)^{S439}], cell migration [cluster of differentiation 244 (CD244)^{S336}, dematin actin-binding protein (DMTN)^{S303}, and myosin IC (MYO1C)^{S408}], and actin cytoskeleton organization [inverted formin-2 (INF2)^{T1179}, DMTN^{S303}, and MYO1C^{S408}]. Kinase substrate enrichment analysis (KSEA) was performed to identify kinase-kinase signaling axes that were enriched in either outcome after COVID-19. The enriched axes were then used to reconstruct kinase networks and ascertain which kinases were crucial for maintaining network integrity (Fig. 5E, left). Analysis revealed the emergence of network dependencies around cyclin-dependent kinase 2 (CDK2), protein kinase C iota (PRKCI), IL-1 receptor–associated kinase 1 (IRAK1), mitogen-activated protein kinase (MEK1), and c-Jun N-terminal kinase 2 (JNK2) in PBMCs derived from individuals with interstitial changes. These kinases are downstream of receptors bound by proinflammatory cytokines (type I IFN and TNF) and regulate

immune pathways required for both T and B cell activation. The kinases responsible for maintaining network integrity in the resolved individuals were more diverse [phosphorylase b kinase gamma catalytic chain, liver/testis isoform, metabolic; proto-oncogene tyrosine-protein kinase Yes, cell growth; ribosomal protein S6 kinase A2, regulates proliferation; Misshapen-like kinase 1, cell adhesion; and numerous others], suggestive of cells that had returned to steady state (Fig. 5E, right). There was also overlap with kinases observed in the interstitial group [such as serine/threonine-protein kinase A-Raf (ARAF)]; however, the underlying ARAF-signaling axes enriched in either group were different. Collectively, these phosphoproteomic data support our findings from the other complimentary -omic approaches whereby signaling in PBMCs from individuals with post–COVID-19 interstitial lung changes are characterized by enrichment for proliferative (CDK2 and MEK1) and immunoregulatory (IRAK1, JNK2, and PRKCI) kinases downstream of receptors to proinflammatory cytokines.

Expression of fibrogenic mediators is up-regulated by exogenous NET administration but not by SARS-CoV-2 infection in human alveolar epithelial cells

We next used in vitro experiments to gain more insight into the drivers of post–COVID-19 interstitial lung changes. Alveolar epithelial cells (AECs) differentiated at the air-liquid interface (Fig. 6A) supported active replication with virus loads increasing from day 0 to day 7 (Fig. 6B) and a detectable innate antiviral immune response indicated by induction of *IFNλ2/3* mRNA (Fig. 6C). Despite this, epithelial SARS-CoV-2 infection did not lead to induction of the prototypical fibrogenic mediators *COL1A*

(collagen 1A) or *FN1* (fibronectin 1) and suppressed expression of *ACTA2* (alpha smooth muscle actin) (Fig. 6D), indicating that live virus infection alone is not sufficient to drive fibrogenesis. To analyze the effect of NET protein on fibrogenic mediators, we then treated A549 epithelial cells with purified NETs (Fig. 6E), which increased mRNA expression of *FN1* and *VEGF* at 24 hours after administration (Fig. 6F). NET administration also altered the expression of genes involved in epithelial-mesenchymal transition, with increased *ACTA2* observed at both 24 and 48 hours after administration and reduced *CDH1* (e-cadherin) observed at 48 hours after administration (Fig. 6G). These findings, coupled with our analyses in human samples, support the conclusion that post–CO-VID-19 interstitial lung disease is driven not only by primary virus infection alone but also by the host inflammatory response to SARS-CoV-2, with NETs being a potential driving factor.

Resolution of interstitial lung changes and associated immune alterations is heterogeneous at 12 months after COVID-19

We next questioned whether post–COVID-19 lung interstitial changes and associated immune alterations resolve over time by assessing longitudinal progression at a second later time point (visit 2; median, 180 days duration between first and second sampling) (Fig. 7A). In the group with interstitial changes, visit 2 data were available for 19 of 26 individuals for % TLCO and 19 of 26 for % FVC. Analysis of change in % TLCO from visit 1 to visit 2 in individuals with interstitial changes as a group indicated overall improvement {median [interquartile range (IQR)] at visit 1: 48.0 (44.0 to 61.0)% versus visit 2: 58.0 (52.5 to 68.4)%; Fig. 7B}. %
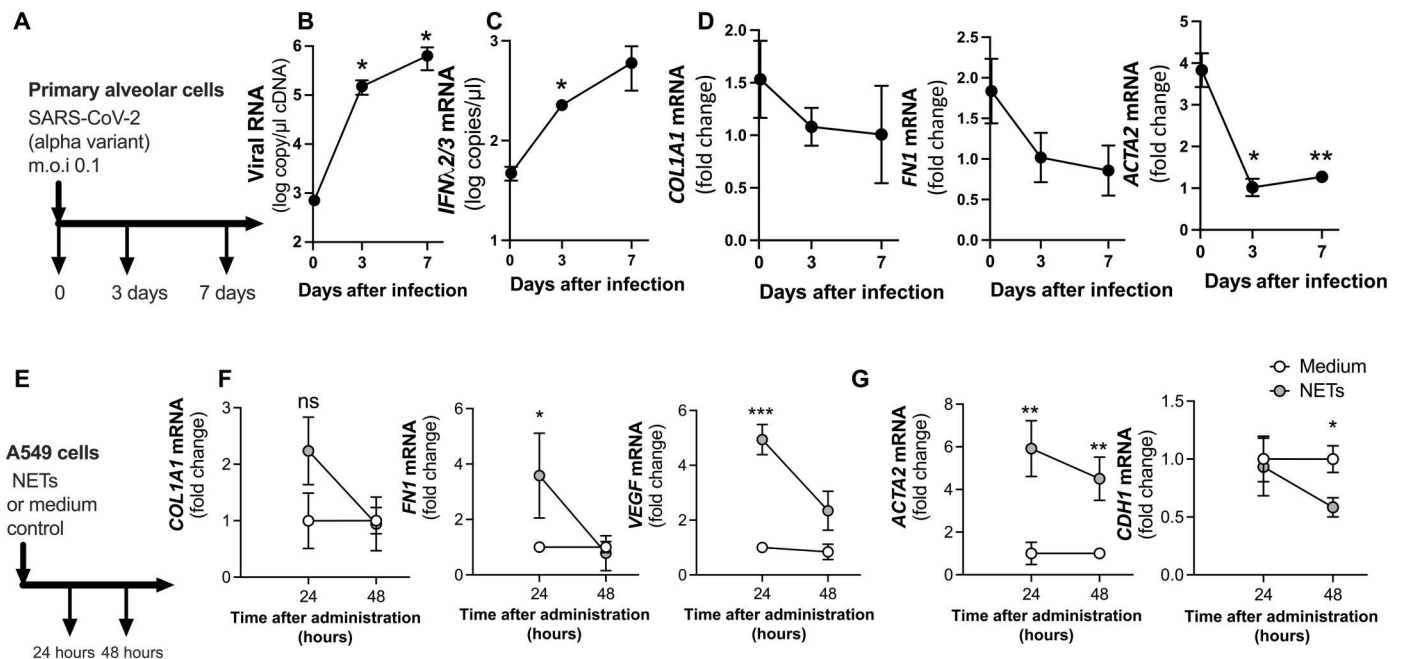
Fig. 6. Exogenous NET administration induces fibrogenic mediators in AECs, an effect not observed with live SARS-CoV-2 infection. (**A**) Experimental timeline of SARS-CoV-2 infection of primary alveolar cells in vitro. (**B**) Viral RNA was measured by quantitative polymerase chain reaction (PCR). (**C**) *IFNλ2/3* and (**D**) *COL1A1, FN1*, and *ACTA2* mRNA expression was measured in primary alveolar cell lysates. (**E**) Experimental timeline of exogenous NET administration to A549 cells in vitro. (**F**) *COL1A1, FN1*, and *VEGF* and (**G**) *ACTA2* and *CDH1* mRNA expression was measured in A549 cell lysates. Data shown as means ± SEM of *n* = 3 biological replicates per group. Data in (B) to (D) were analyzed using ratio paired *t* test with comparison between post-infection and baseline data. Data in (F) and (G) were analyzed using unpaired *t* test with comparison between NETs and medium-treated wells. *$P < 0.05$ and **$P < 0.01$.
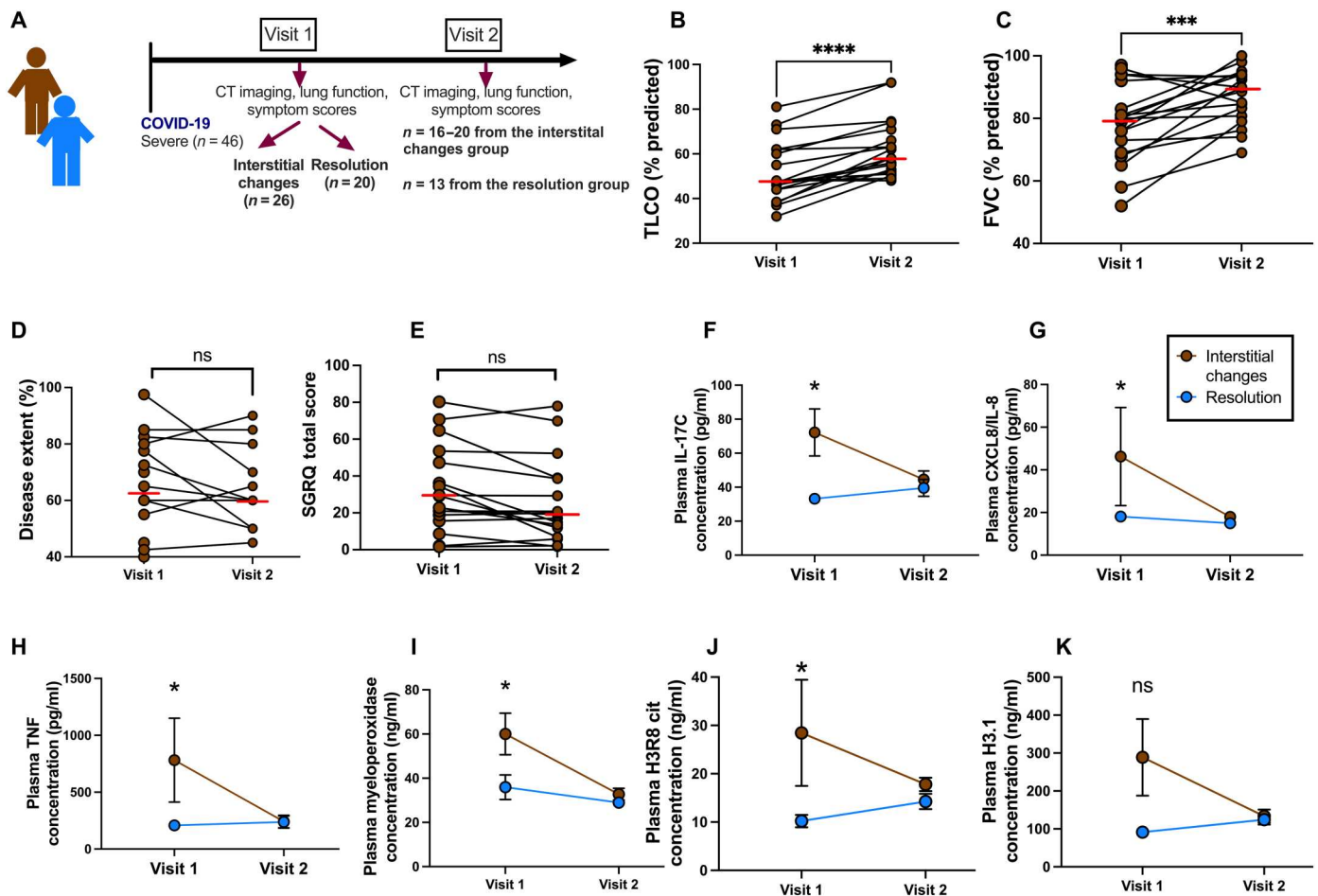
Fig. 7. Resolution of clinical parameters and immune alterations is observed by 12 months after COVID-19. (**A**) Study timeline. (**B**) FVC, (**C**) TLCO, (**D**) radiological disease extent, and (**E**) symptom scores as measured by St. Georges Respiratory Questionnaire (SGRQ) are shown for individuals with interstitial lung changes, and data were collected at the indicated time points after discharge. Plasma concentrations of (**F**) IL-17C, (**G**) CXCL8/IL-8, (**H**) TNF, and (**I**) myeloperoxidase are shown at the indicated time points after discharge. Plasma concentrations of circulating nucleosomes associated with (**J**) H3R8Cit or (**K**) total intact nucleosomes are shown for samples collected at the indicated time points after discharge as measured by H3.1 ELISA. Data in (B) to (E) are shown as individual data points with median indicated by the red line and were analyzed by Wilcoxon rank sum test. Data in (F) to (K) are presented as means ± SEM and were analyzed by Mann-Whitney *U* test to compare the interstitial changes group with the resolution group. *$P < 0.05$, ***$P < 0.001$, and ****$P < 0.0001$.

FVC similarly showed overall improvement in the overall group [median (IQR) at visit 1: 80 (71 to 87.5)% versus visit 2: 89.5 (82.1 to 93.9)%; Fig. 7C]. Despite this overall improvement, 17 of 19 individuals still had TLCO below 75% at visit 2, suggesting that full normalization had not yet occurred in most individuals (although with the caveat that premorbid lung function results are not available, and some may have had preexisting abnormalities). Repeat CT imaging was available in 16 of 26 individuals. Fifteen of 16 subjects still had disease extent of 20% or greater, indicating that full resolution had not yet occurred (Fig. 7D). Repeat St. George's Respiratory Questionnaire scores were available in 17 of 26 individuals and did not show a clear improvement over time (Fig. 7E). This clinical resolution was mirrored by a similar longitudinal reduction of cytokines found to be increased at 3 to 6 months after COVID-19, including TNF, IL-17C, and CXCL8/IL-8 (Fig. 7, F to H) and a similar attenuation in myeloperoxidase, H3.1, and H3R8 nucleosome concentrations (Fig. 7, I to K). Collectively, these data indicate that, in most individuals with

post–COVID-19 interstitial changes evident at 3 to 6 months, partial resolution of clinical and inflammatory abnormalities occurs, although full normalization of lung function and radiographic changes has not yet been reached in many individuals.

DISCUSSION

Using detailed clinical and radiological phenotyping in a cohort of individuals initially hospitalized for severe COVID-19, we define a subgroup of individuals who have persistent morphological and functional changes after recovery from their acute illness. Through multiomic profiling of biological samples taken from the blood and upper airways of these individuals, we elucidated that this complication is characterized by an up-regulated proinflammatory and neutrophil-associated immune signature.

Acute severe COVID-19 is characterized by a proinflammatory signature detectable systematically and in the respiratory tract (*11, 12, 25*). This hyperinflammatory state is believed to drive disease

severity and is amenable to therapeutic inhibition using anti-inflammatory approaches such as dexamethasone (26). Our observations using plasma proteomics to compare individuals hospitalized with severe COVID-19 to those with mild illness indicate that, even after 3 to 6 months after hospital discharge, there is a detectable increase in systemic inflammatory signals. However, it should be noted that variability was evident for some of the analytes, including high values in some healthy individuals (which may represent recent exposure to a viral infection). Our data indicate that severe COVID-19 induces immune activation persisting even after recovery from the acute illness, a finding that is supported by other studies showing similar findings in individuals recovering from acute COVID-19 compared to healthy individuals (18, 27).

Having identified persistent immune activation after severe COVID-19, we next determined whether components of this proinflammatory signature, or alternative pathways, are selectively up-regulated in those with persistent morphologic abnormalities after COVID-19 compared to those showing radiographic resolution. Such comparisons have the potential to offer clearer discrimination of key mechanistic drivers than comparisons to healthy uninfected individuals, as has been the case in other studies (17, 18). We identified a range of increased plasma proteins in individuals with post–COVID-19 interstitial lung changes predominantly consistent with a neutrophil-associated inflammatory signature. Enrichment analysis of immune pathways revealed that "neutrophil chemotaxis" was the most enriched pathway, and a number of differentially expressed proteins were related to neutrophilic inflammation including the chemokine IL-17C (known to have a critical role in regulation of neutrophilic recruitment), the neutrophil-derived cytokine EN-RAGE [recently shown to be expressed in dysfunctional low-density neutrophils in severe COVID-19; (28)], and the proinflammatory cytokines TNF and CCL20. In keeping with this proteomic signature, total blood neutrophil counts were also elevated in individuals with post–COVID-19 interstitial changes. Together, these data indicate that an augmented neutrophil-associated immune signature detectable in the plasma characterizes post–COVID-19 interstitial lung changes.

We additionally sought to determine whether similar changes occurred at the site of initial SARS-CoV-2 infection, the nasal mucosa. We identified a consistent transcriptomic signature in the nasal mucosa of individuals with interstitial lung changes, again at 3 to 6 months after recovery. Differentially expressed genes included the neutrophil chemokine CXCL8, the neutrophil-expressed receptor CXCR2, and the inflammasome-related genes NLRP3 and ILR2. Furthermore, cellular deconvolution analysis revealed an enrichment of neutrophils (but not other cell types) in individuals with post–COVID-19 interstitial lung changes.

The finding of up-regulated systemic and mucosal neutrophil-associated inflammation is consistent with a persistence of this signature from acute disease, with accentuation in those who have persistent abnormalities after COVID-19. Clinical studies in COVID-19 have also reported elevated neutrophil counts in peripheral blood, especially in late-stage disease (29, 30). Higher systemic neutrophil counts and neutrophil chemokine concentrations are also associated with increased disease severity or adverse outcomes (11, 29, 31). Neutrophil chemokine signatures are also up-regulated during acute COVID-19 in airway transcriptomic studies (20). Therefore, ample evidence supports the role played by neutrophils in driving acute severe disease, and our study identifies a role also played in driving the longer-term sequelae of COVID-19. This is reinforced by our finding that systemic neutrophil chemokine (CXCL1/8) concentrations, myeloperoxidase concentrations, and nasal IL17D transcription correlated with radiographic and functional severity. Moreover, after correction for other confounding variables (age, disease severity, requirement for invasive ventilation, and others), plasma concentrations of the neutrophil-regulating cytokine IL-17C remained independently associated with post–COVID-19 interstitial lung changes. IL-17C was also recently shown to be associated with disease progression in non–COVID-19 fibrosing interstitial lung disease (32), which further supports a broader role of this pathway in fibrogenesis.

Effector mechanisms of neutrophils include formation of NETs that comprise networks of fibers composed of DNA containing histones and enzymes (myeloperoxidase and neutrophil elastase) (33). NET formation may have both protective and pathogenic roles; ample evidence indicates roles in propagation of inflammation in a range of conditions, including COVID-19 (34–36), and excessive NET formation can trigger a cascade leading to end-organ damage (37).

Mechanistically, neutrophils may therefore drive fibrogenesis through release of proteases [such as neutrophil elastase and matrix metalloproteinases (MMPs) that can degrade ECM proteins such as types I to IV collagens (38)]. Neutrophil elastase and selected MMPs (MMP-3 and MMP-8) have functional roles in driving bleomycin-induced fibrosis in mice (39–42). Moreover, up-regulation of genes related to pulmonary fibrosis, as well as those for neutrophil activation and NETosis, has been demonstrated in acute fatal COVID-19 (43), further emphasizing the central role of these processes in acute severe disease. In keeping with the hypothesis that NETosis and release of proteases by neutrophils may also drive development of post–COVID-19 interstitial lung changes, we found that patients with this complication had evidence of neutrophilia, increased plasma myeloperoxidase concentrations, and elevated concentrations of intact nucleosomes (as measured by H3.1), as well as increased citrullinated H3R8 nucleosomes. Citrullinated nucleosomes are a major component of NETs as the NETosis process involves nucleosomal histone proteins H3, H2A, and H4 being hypercitrullinated by the enzyme protein arginine deiminase 4 (PAD4). However, PAD4 is dispensable for NETosis, and noncitrullinated NETs are well recognized, although they are less inflammatory than their citrullinated counterparts (44, 45). The functional importance of NETs in driving interstitial changes was indicated by our findings that exogenous administration of purified NETs in an AEC line could induce expression of fibrogenic mediators, an effect not observed with SARS-CoV-2 infection alone, further supporting that the host inflammatory response may be a mechanistically important driver of this complication.

Notably, neutrophil priming and NET formation are poorly responsive to corticosteroids (36) (now widely used for severe COVID-19), emphasizing that alternative approaches are needed. Future functional studies in mouse models of SARS-CoV-2 [including a recently described humanized system that recapitulates pulmonary fibrosis (46) or longitudinal analysis of ongoing clinical trials examining effects of neutrophil-targeting therapies, such as elastase inhibitors (NCT04817332)], upon development of post–COVID-19 interstitial changes, will be required to provide formal confirmation of causal roles.

In addition to an up-regulated neutrophil-associated immune signature detected in the nose, we also identified differentially expressed genes related to augmented antiviral defense pathways. Original thinking related to SARS-CoV-2 infection was that severe disease is associated with impaired type I IFN responses but increased nuclear factor κB–driven proinflammatory responses (*47*). However, increasing evidence indicates greater complexity with airway-focused studies reporting increased IFN-stimulated gene expression occurring concomitantly with proinflammatory genes (*20*). Single-cell sequencing studies in patients with severe COVID-19 have revealed hyperinflammatory immune signatures (including TNF and IL-1β) across all types of immune cells and co-occurring with type I IFN in classical monocytes (*48*). Animal studies have indicated proinflammatory roles for type I IFN during SARS-CoV-2 infection (*49*) with prolonged IFN production after viral infection impairing lung epithelial regeneration (*50*). Our data indicate that post–COVID-19 interstitial changes are associated with a persistence of upper airway type I IFN signature. We interpret that this relates to an initial heightened antiviral response due to increased infection severity (as indicated by greater disease severity, such as requirement for invasive ventilation) observed in the post–COVID-19 interstitial changes group. Our data therefore support a potential mechanism where more severe initial SARS-CoV-2 infection induces a greater type I IFN response; this response then drives subsequent proinflammatory responses with neutrophil NET formation and protease release, potentially leading to ECM degradation and development of interstitial lung changes. NETs are known to signal intracellularly through the cyclic GMP-AMP synthase-Stimulator of interferon genes (cGAS-STING) pathway to release type I IFN (*51*). This pathway has been shown to be activated within the lung tissue of patients with severe COVID-19 and further reinforces the importance of NETs in disease pathogenesis (*52*). It remains unknown at which point therapies would need to be administered to target these pathways and interrupt this process, although some researchers have speculated that this should occur during the early phases of disease (*10*). Whether acute COVID-19 therapies that would suppress type I IFN signaling [such as Janus Kinase (JAK) inhibitors] or neutrophil-mediated inflammation (such as neutrophil elastase inhibitors or extracorporeal removal of NETs through therapeutic apheresis) can effectively reduce the likelihood of long-term pulmonary sequelae requires further study.

To gain a more detailed mechanistic insight into the key alterations in inflammatory signaling pathways, we used phosphoproteomic evaluation of PBMCs, which uncovered a range of kinases enriched in individuals with post–COVID-19 interstitial changes. Consistent with our proteomic and transcriptomic data, a number of these enriched kinases have roles in proinflammatory and neutrophilic pathways, as well as antiviral immunity. These include CDK2 [a canonical cell cycle regulator with roles in neutrophil migration (*53*)], IRAK1 [a component of inflammasome and TLR signaling, as well as type I IFN signaling (*54*, *55*)], and JNK2, which has roles in proinflammatory cytokine responses and neutrophil effector functions (*56*). Moreover, phosphorylation sites increased in individuals with interstitial changes also included proteins implicated in actin cytoskeleton organization. Actin cytoskeleton breakdown is an early feature in the sequence of cellular events occurring in NETosis and precedes plasma and nuclear permeabilization and chromatin decondensation (*57*, *58*). This is consistent with our finding that markers of NETosis are increased in individuals with post–COVID-19 interstitial changes and further supports a potential mechanistic role for neutrophil-associated inflammatory pathways in driving this complication. A range of licensed or late-stage developmental therapies are available that target these kinases and pathways (*59–61*); these approaches may therefore be of future value for ameliorating post–COVID-19 interstitial lung disease.

Sequential evaluation and sampling of our cohort at a second follow-up visit about 6 months after the initial 3- to 6-month assessment indicated that abnormalities in lung function, radiographic changes, and symptom scores show evidence of improvement with time. However, lung function abnormalities, radiological changes, and symptom scores have not fully normalized at this time point (although information about premorbid values for these variables was not available). Whether full normalization of these parameters occurs by a later time point (such as 18 or 24 months) requires future study, and it is unclear whether some individuals will suffer from chronic post–COVID-19 lung fibrosis. The true long-term burden of this complication remains unknown, and results of ongoing large-scale cohort studies are awaited (*62*).

Our study has limitations. First, immune signatures in this study were assessed in peripheral blood and nasal samples. This was a pragmatic approach that allowed sampling to be carried out in a minimally invasive, safe, and cost-effective manner, which also facilitated repeat sampling. However, it should be noted that the primary site of pathology for post–COVID-19 interstitial lung changes is the lower respiratory tract. Although previous studies have shown correlations between nasal and lower airway inflammatory pathways (*63*), it should be acknowledged that there are likely to be anatomical differences in immune expression between these sites that can only be resolved through direct analysis of samples taken directly from the lower airways (such as lavage or biopsies taken using bronchoscopy). Second, although our multiomic analyses identified a number of neutrophil specific readouts, we were unable to undertake a more detailed assessment of neutrophil subphenotypes or activation status. Such analyses cannot be performed retrospectively and would require flow cytometric analysis of fresh blood or airway samples. Third, although our PBMC isolation methods for phosphoproteomic analyses do not formally remove the neutrophils, the freeze-thaw process and wash steps that the samples go through effectively depletes neutrophils and their remnants. We cannot fully exclude the presence of neutrophil debris or lysate within the analyzed PBMCs. Last, although our in vitro studies indicated that NETs may induce expression of fibrogenic mediators in AECs, in vivo formation and activity of NETs are far more complex and are unlikely to be fully recapitulated in our model. Up-regulated expression of fibrogenic mediators indicates a potential for NET-induced pulmonary fibrosis, but further studies using in vivo models will be required for more comprehensive evaluation.

In conclusion, our study uncovers mechanistic insight into the immune pathways driving post–COVID-19 interstitial changes. The longer-term implications of whether chronic changes occur in a subset of these individuals and the potential of targeting neutrophilic inflammation, either in the acute or the recovery phase of COVID-19, to limit disease sequelae require further study.

MATERIALS AND METHODS

Study design

PROSAIC-19 (prospective longitudinal assessment in a COVID-19–infected cohort) is a study prospectively recruiting individuals with COVID-19 confirmed by positive polymerase chain reaction from 1 March 2020 to 1 November 2021. The PROSAIC-19 study aims to comprehensively characterize the long-term pulmonary sequelae of COVID-19 at a clinical and biological level with the ambition of developing interventions that reduce long-term morbidity associated with the disease. There was no intervention, blinding, or randomization conducted as part of study recruitment.

Approvals and participants

The study was approved by the South Central Oxford A Research Ethics Committee (Ref: 20/SC/0208). All participants provided informed written consent. Data were managed using REDCap electronic data capture tools to minimize missing inputs and allow for real-time data validation and quality control. A prespecified case report form was used to prospectively record clinical demographics during acute illness including disease severity, medications, risk factors, and comorbidities at the time of study entry. COVID-19 severity was characterized by the highest seven-category scale during the hospital stay (termed the severity), which consisted of the following categories: 1, not admitted to hospital with resumption of normal activities; 2, not admitted to hospital but unable to resume normal activities; 3, admitted to hospital but not requiring supplemental oxygen; 4, admitted to hospital but requiring supplemental oxygen; 5, admitted to hospital requiring high-flow nasal cannula, noninvasive mechanical ventilation, or both; 6, admitted to hospital requiring extracorporeal membrane oxygenation, invasive mechanical ventilation, or both; and 7, death (64). Participants with scores 5 through 7 were categorized as "severe" disease, and participants with scores 1 to 3 were deemed "mild."

All participants were sampled after hospital discharge at about 3 to 6 months (visit 1), and those with severe disease were invited to attend for further clinical assessment and sampling at about 6 months after this (visit 2). Healthy individuals were recruited as disease controls for the study and sampled once. At baseline and follow-up time points, venous blood sampling and nasal brushings were performed alongside a validated quality-of-life questionnaire (St. George Respiratory Questionnaire). Participants with severe disease had CT chest imaging and pulmonary function tests as part of standard clinical post–COVID-19 follow-up.

Proteomic assays

Plasma proteomic measurements were performed using Olink proximity extension immunoassays (www.olink.com/products/). Two 92-protein multiplex Olink panels were run ("inflammation" and "immune response"), resulting in 184 measurements per sample. Because a small number of proteins (three) were measured on more than one panel, we therefore measured a total of 181 unique proteins. The Olink assays were run using 88 samples per plate. All plates were run in a single batch. Plate layouts were designed to avoid confounding of potential plate effects with biological or clinical variables of interest ensuring case/control balance across plates with random selection of samples from each category and random ordering of allocation to wells. Specifically, a fixed proportion of each plate was designated for control samples. The data were normalized using standard Olink workflows to produce relative protein abundance on a $\log_2$ scale ("NPX"). Quality assessment was performed by (i) examination of Olink internal controls and (ii) inspection of boxplots, relative log expression plots (65), and principal component analysis.

Nanostring nCounter analysis

Total RNA was extracted from nasal brush samples using a Qiagen RNAeasy kit following the manufacturer's instructions. Nanostring profiling of host response was performed using the nCounter Human Host Response Panel. Total RNA (50 ng) was hybridized to reporter and capture probe sets at 65°C for 24 hours. Probe set–target RNA complexes were purified and immobilized on nCounter Cartridges using an nCounter Prep Station (3 hours and 20 min total time). Data collection was carried out in the nCounter Digital Analyzer; at the highest standard data resolution, 555 fields of view were collected (6 hours total time) per flow cell using a microscope objective and a charge-coupled device camera yielding data of all the target molecule counts. Raw data were preprocessed using both nSolver 2.0 software (Nanostring Technologies) and the Rosalind packages. Preprocessing sequentially corrects for three factors: technical variation, background, and sample content. First, using a set of exogenous positive control RNAs present in each sample, technical variation was accounted for by adjusting the counts in each sample to the geometric mean of counts for positive control counts in all samples. Subsequently, a background correction was performed by subtracting the maximum count value of the negative control probes in a sample from each probe output within the sample. Transcript counts that were negative after background correction were set to 1. Each sample was then normalized for RNA content by adjusting the counts to the geometric mean of 15 housekeeping genes. Last, the data were $\log_2$-transformed. Network data were designed by association matrix, and the graph file was created using Gephi. Nodes were aligned by Force Atlas algorithm, and the centrality was calculated by the betweenness. Downstream statistical analyses were performed using GraphPad Prism version 9.0.

Phosphoproteomic assays

PBMCs (3×10^6) were washed with phosphate-buffered saline (PBS) and lysed with a buffer containing 8 M urea in 20 mM Hepes (pH 8) supplemented with 1 mM Na_3VO_4, 1 mM NaF, 1 mM Na β-glycerol phosphate, and 2.5 mM $Na_2H_2P_2O_7$. The resultant lysates were then processed as previously described (66). Briefly, samples were sonicated and normalized to 110 μg of protein through the use of a Pierce bicinchoninic acid assay, following which samples were subjected to tryptic digestion before desalting and phosphoenrichment.

Enriched phosphopeptides were loaded onto a liquid chromatography with a tandem mass spectrometry (LC-MS/MS) system consisting of Dionex UltiMate 3000 rapid separation liquid chromatography directly coupled to an Orbitrap Q-Exactive Plus mass spectrometer (Thermo Fisher Scientific). The LC method comprised mobile phases A [3% Acetonitrile ACN; 0.1% Formic Acid (FA)] and B (100% ACN; 0.1% FA). Peptides were trapped on a μ-precolumn (Thermo Fisher Scientific) at a flow rate of 10 μl/min and separated on a 50-cm EASY-Spray (Thermo Fisher Scientific) LC Column with a gradient of 3 to 23% B (across 90 min) and a flow rate of 0.3 μl/min. The mass spectrometer operated with a 2.1-s duty cycle. MS1 survey spectra [mass-to-charge ratio (m/z) 375 to

George et al., Sci. Transl. Med. 14, eabo5795 (2022)   16 November 2022

12 of 16

1500] were acquired with a resolution of 70,000 and followed a data-dependent acquisition method in which the 10 most intense ions were selected for fragmentation; subsequent fragments (MS2; scanning 200 to 2000 *m/z*) were acquired with a resolution of 17,500. Dynamic exclusion was set to 30 s.

Peptide identification steps systematically searched LC-MS/MS data against the SwissProt human database using Mascot 2.5 (Matrix Science) (*67*). Allowable peptide modifications included phospho-Ser (S), phospho-Thr (T), phospho-Tyr (Y), oxidized Met (M), and pyro-Glu (Q). Phosphopeptide intensities were quantified in each sample through the use of in-house PiQuant software. Missing values were imputed using a multiple imputation strategy. In brief, this involves imputation of missing-completely-at-random values with a maximum likelihood estimator approach, followed by imputation of missing-not-at-random values with an imputation under a Gaussian complete data assumption approach. Data were then scale-normalized, and differential expression analysis was performed through the fitting of an empirical Bayes linear model (*68*). The prior probability for differential expression was set at 1%. A posterior probability of differential expression greater than 0.99 (translating to a log OR above 4.599) was considered strong evidence of differential expression. Where provided in the differential expression analyses, *P* values were adjusted for multiple testing through the use of the Benjamini-Yekutieli procedure. Kinase activities from the phosphoproteomics data were calculated using KSEA as described previously (*69*, *70*).

Infection of AECs with SARS-CoV-2
Before infection, cells were washed once with PBS. Cells were inoculated in triplicate with SARS-CoV-2 alpha variant at 0.1 multiplicity of infection or media control, diluted in 250 μl of bronchial epithelial cell growth basal medium, on the apical surface only. After 2 hours of incubation at 37°C, the inoculum was removed, and unbound virus was washed off using 500 μl of PBS, corresponding to the beginning of the time course. AECs were harvested at 3 and 7 days after infection to measure cellular viral RNA, immune mRNA, and fibrotic mRNA. Upon harvest, apical washes were collected by the addition of 500 μl of PBS for 5 min. Cells were collected in RNA lysis (RLT) buffer (Qiagen) containing 1% 2-mercaptoethanol for total RNA extraction.

Generation of NETs and administration in A549 cells
NETs were generated as previously described (*71*). In brief, dimethyl sulfoxide–differentiated HL60 neutrophils were incubated in Dulbecco's modified Eagle's medium (DMEM) and stimulated with 100 nM phorbol 12-myristate 13-acetate (PMA) for 5 hours. The medium was removed and centrifuged for 5 min at 10,000*g* to remove cells and cellular debris. Two milliliters of HL-60 PMA-stimulated media or standard DMEM + 100 nM PMA was added to submerged A549 cells (American Tissue Culture Collection Catalog number CCL-185) and incubated at 37°C with 5% CO_2. Cell lysates were collected in RLT buffer (Qiagen) at 24 and 48 hours after administration.

Data analysis
Raw, individual-level data for experiments where $n < 20$ are presented in data file S1. Data from human samples were analyzed using the Mann-Whitney *U* test (≤2 groups) or the Kruskal-Wallis test with Dunn's posttest (>2 groups). Correlations between datasets were examined using Spearman's rank correlation coefficient. All statistics were performed using GraphPad Prism 8 software. Differences were considered significant when $P < 0.05$.

Supplementary Materials
This PDF file includes:
Figs. S1 to S3
Table S1 to S3
References (*72*, *73*)

Other Supplementary Material for this manuscript includes the following:
Data file S1
MDAR Reproducibility Checklist

View/request a protocol for this paper from *Bio-protocol*.

REFERENCES AND NOTES
1. A. B. Docherty, E. M. Harrison, C. A. Green, H. E. Hardwick, R. Pius, L. Norman, K. A. Holden, J. M. Read, F. Dondelinger, G. Carson, L. Merson, J. Lee, D. Plotkin, L. Sigfrid, S. Halpin, C. Jackson, C. Gamble, P. W. Horby, J. S. Nguyen-Van-Tam, A. Ho, C. D. Russell, J. Dunning, P. J. Openshaw, J. K. Baillie, M. G. Semple; ISARIC4C investigators, Features of 20 133 UK patients in hospital with covid-19 using the ISARIC WHO Clinical Characterisation Protocol: Prospective observational cohort study. *BMJ* **369**, m1985 (2020).
2. R. A. Evans, H. M. Auley, E. M. Harrison, A. Shikotra, A. Singapuri, M. Sereno, O. Elneima, A. B. Docherty, N. I. Lone, O. C. Leavy, L. Daines, J. K. Baillie, J. S. Brown, T. Chalder, A. De Soyza, N. D. Bakerly, N. Easom, J. R. Geddes, N. J. Greening, N. Hart, L. G. Heaney, S. Heller, L. Howard, J. R. Hurst, J. Jacob, R. G. Jenkins, C. Jolley, S. Kerr, O. M. Kon, K. Lewis, J. M. Lord, G. P. M. Cann, S. Neubauer, P. J. M. Openshaw, D. Parekh, P. Pfeffer, N. M. Rahman, B. Raman, M. Richardson, M. Rowland, M. G. Semple, A. M. Shah, S. J. Singh, A. Sheikh, D. Thomas, M. Toshner, J. D. Chalmers, L.-P. Ho, A. Horsley, M. Marks, K. Poinasamy, L. V. Wain, C. E. Brightling; on behalf of thePHOSP-COVID Collaborative Group, Physical, cognitive, and mental health impacts of COVID-19 after hospitalisation (PHOSP-COVID): A UK multicentre, prospective cohort study. *The Lancet Respir. Med.* **9**, 1275–1287 (2021).
3. M. Augustin, P. Schommers, M. Stecher, F. Dewald, L. Gieselmann, H. Gruell, C. Horn, K. Vanshylla, V. D. Cristanziano, L. Osebold, M. Roventa, T. Riaz, N. Tschernoster, J. Altmueller, L. Rose, S. Salomon, V. Priesner, J. C. Luers, C. Albus, S. Rosenkranz, B. Gathof, G. Fatkenheuer, M. Hallek, F. Klein, I. Suarez, C. Lehmann, Post-COVID syndrome in non-hospitalised patients with COVID-19: A longitudinal prospective cohort study. *Lancet Reg. Health Eur.* **6**, 100122 (2021).
4. A. Nalbandian, K. Sehgal, A. Gupta, M. V. Madhavan, C. McGroder, J. S. Stevens, J. R. Cook, A. S. Nordvig, D. Shalev, T. S. Sehrawat, N. Ahluwalia, B. Bikdeli, D. Dietz, C. Der-Nigoghossian, N. Liyanage-Don, G. F. Rosner, E. J. Bernstein, S. Mohan, A. A. Beckley, D. S. Seres, T. K. Choueiri, N. Uriel, J. C. Ausiello, D. Accili, D. E. Freedberg, A. Schwartz, D. Brodie, C. K. Garcia, M. S. V. Elkind, J. M. Connors, J. P. Bilezikian, D. W. Landry, E. Y. Wan, Post-acute COVID-19 syndrome. *Nat. Med.* **27**, 601–615 (2021).
5. X. Han, Y. Fan, O. Alwalid, N. Li, X. Jia, M. Yuan, Y. Li, Y. Cao, J. Gu, H. Wu, H. Shi, Six-month follow-up chest CT findings after severe COVID-19 pneumonia. *Radiology* **299**, E177–E186 (2021).
6. S. A. Guler, L. Ebner, C. Aubry-Beigelman, P. O. Bridevaux, M. Brutsche, C. Clarenbach, C. Garzoni, T. K. Geiser, A. Lenoir, M. Mancinetti, B. Naccini, S. R. Ott, L. Piquilloud, M. Prella, Y. A. Que, P. M. Soccal, C. von Garnier, M. Funke-Chambour, Pulmonary function and radiological features 4 months after COVID-19: First results from the national prospective observational Swiss COVID-19 lung study. *Eur. Respir. J.* **57**, 2003690 (2021).
7. Y.-H. Xu, J.-H. Dong, W.-M. An, X.-Y. Lv, X.-P. Yin, J.-Z. Zhang, L. Dong, X. Ma, H.-J. Zhang, B.-L. Gao, Clinical and computed tomographic imaging features of novel coronavirus pneumonia caused by SARS-CoV-2. *J. Infect.* **80**, 394–400 (2020).
8. X. Mo, W. Jian, Z. Su, M. Chen, H. Peng, P. Peng, C. Lei, R. Chen, N. Zhong, S. Li, Abnormal pulmonary function in COVID-19 patients at time of hospital discharge. *Eur. Respir. J.* **55**, 2001217 (2020).
9. X. Li, C. Shen, L. Wang, S. Majumder, D. Zhang, M. J. Deen, Y. Li, L. Qing, Y. Zhang, C. Chen, R. Zou, J. Lan, L. Huang, C. Peng, L. Zeng, Y. Liang, M. Cao, Y. Yang, M. Yang, G. Tan, S. Tang, L. Liu, J. Yuan, Y. Liu, Pulmonary fibrosis and its related factors in discharged patients with new corona virus pneumonia: A cohort study. *Respir. Res.* **22**, 203 (2021).
10. P. M. George, A. U. Wells, R. G. Jenkins, Pulmonary fibrosis and COVID-19: The potential role for antifibrotic therapy. *Lancet Respir. Med.* **8**, 807–815 (2020).

11. R. S. Thwaites, A. S. S. Uruchurtu, M. K. Siggins, F. Liew, C. D. Russell, S. C. Moore, C. Fairfield, E. Carter, S. Abrams, C. E. Short, T. Thaventhiran, E. Bergstrom, Z. Gardener, S. Ascough, C. Chiu, A. B. Docherty, D. Hunt, Y. J. Crow, T. Solomon, G. P. Taylor, L. Turtle, E. M. Harrison, J. Dunning, M. G. Semple, J. K. Baillie, P. J. Openshaw; ISARIC4C investigators, Inflammatory profiles across the spectrum of disease reveal a distinct role for GM-CSF in severe COVID-19. *Sci. Immunol.* **6**, eabg9873 (2021).

12. J. C. Melms, J. Biermann, H. Huang, Y. Wang, A. Nair, S. Tagore, I. Katsyv, A. F. Rendeiro, A. D. Amin, D. Schapiro, C. J. Frangieh, A. M. Luoma, A. Filliol, Y. Fang, H. Ravichandran, M. G. Clausi, G. A. Alba, M. Rogava, S. W. Chen, P. Ho, D. T. Montoro, A. E. Kornberg, A. S. Han, M. F. Bakhoum, N. Anandasabapathy, M. Suárez-Fariñas, S. F. Bakhoum, Y. Bram, A. Borczuk, X. V. Guo, J. H. Lefkowitch, C. Marboe, S. M. Lagana, A. D. Portillo, E. J. Tsai, E. Zorn, G. S. Markowitz, R. F. Schwabe, R. E. Schwartz, O. Elemento, A. Saqi, H. Hibshoosh, J. Que, B. Izar, A molecular single-cell lung atlas of lethal COVID-19. *Nature* **595**, 114–119 (2021).

13. A. F. Rendeiro, H. Ravichandran, Y. Bram, V. Chandar, J. Kim, C. Meydan, J. Park, J. Foox, T. Hether, S. Warren, Y. Kim, J. Reeves, S. Salvatore, C. E. Mason, A. C. Swanson, A. C. Borczuk, O. Elemento, R. E. Schwartz, The spatial landscape of lung pathology during COVID-19 progression. *Nature* **593**, 564–569 (2021).

14. E. R. Mann, M. Menon, S. B. Knight, J. E. Konkel, C. Jagger, T. N. Shaw, S. Krishnan, M. Rattray, A. Ustianowski, N. D. Bakerly, P. Dark, G. Lord, A. Simpson, T. Felton, L. P. Ho, N. R. TRC, M. Feldmann; CIRCO, J. R. Grainger, T. Hussell, Longitudinal immune profiling reveals key myeloid signatures associated with COVID-19. *Sci. Immunol.* **5**, eabd6197 (2020).

15. R. A. Grant, L. Morales-Nebreda, N. S. Markov, S. Swaminathan, M. Querrey, E. R. Guzman, D. A. Abbott, H. K. Donnelly, A. Donayre, I. A. Goldberg, Z. M. Klug, N. Borkowski, Z. Lu, H. Kihshen, Y. Politanska, L. Sichizya, M. Kang, A. Shilatifard, C. Qi, J. W. Lomasney, A. C. Argento, J. M. Kruser, E. S. Malsin, C. O. Pickens, S. B. Smith, J. M. Walter, A. E. Pawlowski, D. Schneider, P. Nannapaneni, H. Abdala-Valencia, A. Bharat, C. J. Gottardi, G. R. S. Budinger, A. V. Misharin, B. D. Singer, R. G. Wunderink; NU SCRIPT Study Investigators, Circuits between infected macrophages and T cells in SARS-CoV-2 pneumonia. *Nature* **590**, 635–641 (2021).

16. D. A. Dorward, C. D. Russell, I. H. Um, M. Elshani, S. D. Armstrong, R. Penrice-Randal, T. Millar, C. E. B. Lerpiniere, G. Tagliavini, C. S. Hartley, N. P. Randle, N. N. Gachanja, P. M. D. Potey, X. Dong, A. M. Anderson, V. L. Campbell, A. J. Duguid, W. Al Qsous, R. BouHaidar, J. K. Baillie, K. Dhaliwal, W. A. Wallace, C. O. C. Bellamy, S. Prost, C. Smith, J. A. Hiscox, D. J. Harrison, C. D. Lucas, Tissue-specific immunopathology in fatal COVID-19. *Am. J. Respir. Crit. Care Med.* **203**, 192–201 (2021).

17. I. S. Cheon, C. Li, Y. M. Son, N. P. Goplen, Y. Wu, T. Cassmann, Z. Wang, X. Wei, J. Tang, Y. Li, H. Marlow, S. Hughes, L. Hammel, T. M. Cox, E. Goddery, K. Ayasoufi, D. Weiskopf, J. Boonyaratanakornkit, H. Dong, H. Li, R. Chakraborty, A. J. Johnson, E. Edell, J. J. Taylor, M. H. Kaplan, A. Sette, B. J. Bartholmai, R. Kern, R. Vassallo, J. Sun, Immune signatures underlying post-acute COVID-19 lung sequelae. *Sci. Immunol.* **6**, eabk1741 (2021).

18. B. Vijayakumar, K. Boustani, P. P. Ogger, A. Papadaki, J. Tonkin, C. M. Orton, P. Ghai, K. Suveizdyte, R. J. Hewitt, S. R. Desai, A. Devaraj, R. J. Snelgrove, P. L. Molyneaux, J. L. Garner, J. E. Peters, P. L. Shah, C. M. Lloyd, J. A. Harker, Immuno-proteomic profiling reveals aberrant immune cell regulation in the airways of individuals with ongoing post-COVID-19 respiratory disease. *Immunity* **55**, 542–556.e5 (2022).

19. M. Selman, A. Pardo, When things go wrong: Exploring possible mechanisms driving the progressive fibrosis phenotype in interstitial lung diseases. *Eur. Respir. J.* **58**, 2004507 (2021).

20. Z. Zhou, L. Ren, L. Zhang, J. Zhong, Y. Xiao, Z. Jia, L. Guo, J. Yang, C. Wang, S. Jiang, D. Yang, G. Zhang, H. Li, F. Chen, Y. Xu, M. Chen, Z. Gao, J. Yang, J. Dong, B. Liu, X. Zhang, W. Wang, K. He, Q. Jin, M. Li, J. Wang, Heightened innate immune responses in the respiratory tract of COVID-19 patients. *Cell Host Microbe* **27**, 883–890.e2 (2020).

21. B. Sposito, A. Broggi, L. Pandolfi, S. Crotta, N. Clementi, R. Ferrarese, S. Sisti, E. Criscuolo, R. Spreafico, J. M. Long, A. Ambrosi, E. Liu, V. Frangipane, L. Saracino, S. Bozzini, L. Marongiu, F. A. Facchini, A. Bottazzi, T. Fossali, R. Colombo, M. Clementi, E. Tagliabue, J. Chou, A. E. Pontiroli, F. Meloni, A. Wack, N. Mancini, I. Zanoni, The interferon landscape along the respiratory tract impacts the severity of COVID-19. *Cell* **184**, 4953–4968.e16 (2021).

22. C. F. Hatton, R. A. Botting, M. E. Duenas, I. J. Haq, B. Verdon, B. J. Thompson, J. S. Spegarova, F. Gothe, E. Stephenson, A. I. Gardner, S. Murphy, J. Scott, J. P. Garnett, S. Carrie, J. Powell, C. M. A. Khan, L. Huang, R. Hussain, J. Coxhead, T. Davey, A. J. Simpson, M. Haniffa, S. Hambleton, M. Brodlie, C. Ward, M. Trost, G. Reynolds, C. J. A. Duncan, Delayed induction of type I and III interferons mediates nasal epithelial cell permissiveness to SARS-CoV-2. *Nat. Commun.* **12**, 7092 (2021).

23. A. Park, A. Iwasaki, Type I and type III interferons—Induction, signaling, evasion, and application to combat COVID-19. *Cell Host Microbe* **27**, 870–878 (2020).

24. L. Zhang, S.-Y. Lu, R. Guo, J.-X. Ma, L.-Y. Tang, J.-J. Wang, C.-L. Shen, L.-M. Lu, J. Liu, Z.-G. Wang, H.-X. Zhang, STK10 knockout inhibits cell migration and promotes cell proliferation via modulating the activity of ERM and p38 MAPK in prostate cancer cells. *Exp. Ther. Med.* **22**, 851 (2021).

25. A. F. Rendeiro, H. Ravichandran, Y. Bram, S. Salvatore, A. Borczuk, O. Elemento, R. E. Schwartz, The spatio-temporal landscape of lung pathology in SARS-CoV-2 infection. *medRxiv*, 10.1101/2020.10.26.20219584 , (2020).

26. RECOVERY Collaborative Group, P. Horby, W. S. Lim, J. R. Emberson, M. Mafham, J. L. Bell, L. Linsell, N. Staplin, C. Brightling, A. Ustianowski, E. Elmahi, B. Prudon, C. Green, T. Felton, D. Chadwick, K. Rege, C. Fegan, L. C. Chappell, S. N. Faust, T. Jaki, K. Jeffery, A. Montgomery, K. Rowan, E. Juszczak, J. K. Baillie, R. Haynes, M. J. Landray, Dexamethasone in hospitalized patients with Covid-19. *N. Engl. J. Med.* **384**, 693–704 (2021).

27. S. W. X. Ong, S.-W. Fong, B. E. Young, Y.-H. Chan, B. Lee, S. N. Amrun, R. S.-L. Chee, N. K.-W. Yeo, P. Tambyah, S. Pada, S. Y. Tan, Y. Ding, L. Renia, Y.-S. Leo, L. F. P. Ng, D. C. Lye, Persistent symptoms and association with inflammatory cytokine signatures in recovered coronavirus disease 2019 patients. *Open Forum Infect. Dis.* **8**, ofab156 (2021).

28. J. Schulte-Schrepping, N. Reusch, D. Paclik, K. Baßler, S. Schlickeiser, B. Zhang, B. Kramer, T. Krammer, S. Brumhard, L. Bonaguro, E. De Domenico, D. Wendisch, M. Grasshoff, T. S. Kapellos, M. Beckstette, T. Pecht, A. Saglam, O. Dietrich, H. E. Mei, A. R. Schulz, C. Conrad, D. Kunkel, E. Vafadarnejad, C.-J. Xu, A. Horne, M. Herbert, A. Drews, C. Thibeault, M. Pfeiffer, S. Hippenstiel, A. Hocke, H. Müller-Redetzky, K. M. Heim, F. Machleidt, A. Uhrig, L. B. de Jarcy, L. Jürgens, M. Stegemann, C. R. Glösenkamp, H.-D. Volk, C. Goffinet, M. Landthaler, E. Wyler, P. Georg, M. Schneider, C. Dang-Heine, N. Neuwinger, K. Kappert, R. Tauber, V. Corman, J. Raabe, K. M. Kaiser, M. T. Vinh, G. Rieke, C. Meisel, T. Ulas, M. Becker, R. Geffers, M. Witzenrath, C. Drosten, N. Suttorp, C. von Kalle, F. Kurth, K. Handler, J. L. Schultze, A. C. Aschenbrenner, Y. Li, J. Nattermann, B. Sawitzki, A.-E. Saliba, L. E. Sander; Deutsche COVID-19 OMICS Initiative (DeCOI), Severe COVID-19 is marked by a dysregulated myeloid cell compartment. *Cell* **182**, 1419–1440.e23 (2020).

29. D. Huang, X. Lian, F. Song, H. Ma, Z. Lian, Y. Liang, T. Qin, W. Chen, S. Wang, Clinical features of severe patients infected with 2019 novel coronavirus: A systematic review and meta-analysis. *Ann. Transl. Med.* **8**, 576 (2020).

30. D. Wang, B. Hu, C. Hu, F. Zhu, X. Liu, J. Zhang, B. Wang, H. Xiang, Z. Cheng, Y. Xiong, Y. Zhao, Y. Li, X. Wang, Z. Peng, Clinical characteristics of 138 hospitalized patients with 2019 novel coronavirus-infected pneumonia in Wuhan, China. *JAMA* **323**, 1061–1069 (2020).

31. O. J. McElvaney, N. L. McEvoy, O. F. McElvaney, T. P. Carroll, M. P. Murphy, D. M. Dunlea, O. N. Choileain, J. Clarke, E. O'Connor, G. Hogan, D. Ryan, I. Sulaiman, C. Gunaratnam, P. Branagan, M. E. O'Brien, R. K. Morgan, R. W. Costello, K. Hurley, S. Walsh, E. de Barra, C. McNally, S. McConkey, F. Boland, S. Galvin, F. Kiernan, J. O'Rourke, R. Dwyer, M. Power, P. Geoghegan, C. Larkin, R. A. O'Leary, J. Freeman, A. Gaffney, B. Marsh, G. F. Curley, N. G. McElvaney, Characterization of the inflammatory response to severe COVID-19 illness. *Am. J. Respir. Crit. Care Med.* **202**, 812–821 (2020).

32. W. S. Bowman, C. A. Newton, A. L. Linderholm, M. L. Neely, J. V. Pugashetti, B. Kaul, V. Vo, G. A. Echt, W. Leon, R. J. Shah, Y. Huang, C. K. Garcia, P. J. Wolters, J. M. Oldham, Proteomic biomarkers of progressive fibrosing interstitial lung disease: A multicentre cohort analysis. *Lancet Respir. Med.* **10**, 593–602 (2022).

33. V. Brinkmann, U. Reichard, C. Goosmann, B. Fauler, Y. Uhlemann, D. S. Weiss, Y. Weinrauch, A. Zychlinsky, Neutrophil extracellular traps kill bacteria. *Science* **303**, 1532–1535 (2004).

34. Y. Zuo, S. Yalavarthi, H. Shi, K. Gockman, M. Zuo, J. A. Madison, C. Blair, A. Weber, B. J. Barnes, M. Egeblad, R. J. Woods, Y. Kanthi, J. S. Knight, Neutrophil extracellular traps in COVID-19. *JCI Insight* **5**, e138999 (2020).

35. F. P. Veras, M. C. Pontelli, C. M. Silva, J. E. Toller-Kawahisa, M. de Lima, D. C. Nascimento, A. H. Schneider, D. Caetite, L. A. Tavares, I. M. Paiva, R. Rosales, D. Colon, R. Martins, I. A. Castro, G. M. Almeida, M. I. F. Lopes, M. N. Benatti, L. P. Bonjorno, M. C. Giannini, R. Luppino-Assad, S. L. Almeida, F. Vilar, R. Santana, V. R. Bollela, M. Auxiliadora-Martins, M. Borges, C. H. Miranda, A. Pazin-Filho, L. L. P. da Silva, L. D. Cunha, D. S. Zamboni, F. Dal-Pizzol, L. O. Leiria, L. Siyuan, S. Batah, A. Fabro, T. Mauad, M. Dolhnikoff, A. Duarte-Neto, P. Saldiva, T. M. Cunha, J. C. Alves-Filho, E. Arruda, P. Louzada-Junior, R. D. Oliveira, F. Q. Cunha, SARS-CoV-2-triggered neutrophil extracellular traps mediate COVID-19 pathology. *J. Exp. Med.* **217**, e20201129 (2020).

36. R. Panda, F. V. Castanheira, J. M. Schlechte, B. G. Surewaard, H. B. Shim, A. Z. Zucoloto, Z. Slavikova, B. G. Yipp, P. Kubes, B. McDonald, A functionally distinct neutrophil landscape in severe COVID-19 reveals opportunities for adjunctive therapies. *JCI Insight* **7**, e152291 (2021).

37. B. J. Barnes, J. M. Adrover, A. Baxter-Stoltzfus, A. Borczuk, J. Cools-Lartigue, J. M. Crawford, J. Daßler-Plenker, P. Guerci, C. Huynh, J. S. Knight, M. Loda, M. R. Looney, F. McAllister, R. Rayes, S. Renaud, S. Rousseau, S. Salvatore, R. E. Schwartz, J. D. Spicer, C. C. Yost, A. Weber, Y. Zuo, M. Egeblad, Targeting potential drivers of COVID-19: Neutrophil extracellular traps. *J. Exp. Med.* **217**, e20200652 (2020).

38. K. T. Mincham, N. Bruno, A. Singanayagam, R. J. Snelgrove, Our evolving view of neutrophils in defining the pathology of chronic lung disease. *Immunology* **164**, 701–721 (2021).

39. F. Chua, S. E. Dunsmore, P. H. Clingen, S. E. Mutsaers, S. D. Shapiro, A. W. Segal, J. Roes, G. J. Laurent, Mice lacking neutrophil elastase are resistant to bleomycin-induced pulmonary fibrosis. *Am. J. Pathol.* **170**, 65–74 (2007).

George *et al.*, *Sci. Transl. Med.* **14**, eabo5795 (2022) 16 November 2022

14 of 16

40. A. Takemasa, Y. Ishii, T. Fukuda, A neutrophil elastase inhibitor prevents bleomycin-induced pulmonary fibrosis in mice. *Eur. Respir. J.* **40**, 1475–1482 (2012).

41. C. M. Yamashita, L. Dolgonos, R. L. Zemans, S. K. Young, J. Robertson, N. Briones, T. Suzuki, M. N. Campbell, J. Gauldie, D. C. Radisky, D. W. Riches, G. Yu, N. Kaminski, C. A. McCulloch, G. P. Downey, Matrix metalloproteinase 3 is a mediator of pulmonary fibrosis. *Am. J. Pathol.* **179**, 1733–1745 (2011).

42. E. García-Prieto, A. González-López, S. Cabrera, A. Astudillo, A. Gutiérrez-Fernández, M. Fanjul-Fernandez, E. Batalla-Solís, X. S. Puente, A. Fueyo, C. López-Otín, G. M. Albaiceta, Resistance to bleomycin-induced lung fibrosis in MMP-8 deficient mice is mediated by interleukin-10. *PLOS ONE* **5**, e13242 (2010).

43. M. Wu, Y. Chen, H. Xia, C. Wang, C. Y. Tan, X. Cai, Y. Liu, F. Ji, P. Xiong, R. Liu, Y. Guan, Y. Duan, D. Kuang, S. Xu, H. Cai, Q. Xia, D. Yang, M.-W. Wang, I. M. Chiu, C. Cheng, P. P. Ahern, L. Liu, G. Wang, N. K. Surana, T. Xia, D. L. Kasper, Transcriptional and proteomic insights into the host response in fatal COVID-19 cases. *Proc. Natl. Acad. Sci. U.S.A.* **117**, 28336–28343 (2020).

44. T.-D. Tsourouktsoglou, A. Warnatsch, M. Ioannou, D. Hoving, Q. Wang, V. Papayannopoulos, Histones, DNA, and citrullination promote neutrophil extracellular trap inflammation by regulating the localization and activation of TLR4. *Cell Rep.* **31**, 107602 (2020).

45. J. Huckriede, F. de Vries, M. Hultstrom, K. Wichapong, C. Reutelingsperger, M. Lipcsey, P. Garcia de Frutos, R. Frithiof, G. A. F. Nicolaes, Histone H3 cleavage in severe COVID-19 ICU patients. *Front. Cell. Infect. Microbiol.* **11**, 694186 (2021).

46. K. H. Dinnon III, S. R. Leist, K. Okuda, H. Dang, E. J. Fritch, K. L. Gully, G. De la Cruz, M. D. Evangelista, T. Asakura, R. C. Gilmore, P. Hawkins, S. Nakano, A. West, A. Schäfer, L. E. Gralinski, J. L. Everman, S. P. Sajuthi, M. R. Zweigart, S. Dong, J. McBride, M. R. Cooley, J. B. Hines, M. K. Love, S. D. Groshong, A. VanSchoiack, S. J. Phelan, Y. Liang, T. Hether, M. Leon, R. E. Zumwalt, L. M. Barton, E. J. Duval, S. Mukhopadhyay, E. Stroberg, A. Borczuk, L. B. Thorne, M. K. Sakthivel, Y. Z. Lee, J. S. Hagood, J. R. Mock, M. A. Seibold, W. K. O'Neal, S. A. Montgomery, R. C. Boucher, R. S. Baric, SARS-CoV-2 infection produces chronic pulmonary epithelial and immune cell dysfunction with fibrosis in mice. *Sci. Transl. Med.* **14**, eabo5070 (2022).

47. J. Hadjadj, N. Yatim, L. Barnabei, A. Corneau, J. Boussier, N. Smith, H. Peré, B. Charbit, V. Bondet, C. Chenevier-Gobeaux, P. Breillat, N. Carlier, R. Gauzit, C. Morbieu, F. Pene, N. Marin, N. Roche, T.-A. Szwebel, S. H. Merkling, J. M. Treluyer, D. Veyer, L. Mouthon, C. Blanc, P.-L. Tharaux, F. Rozenberg, A. Fischer, D. Duffy, F. Rieux-Laucat, S. Kernéis, B. Terrier, Impaired type I interferon activity and inflammatory responses in severe COVID-19 patients. *Science* **369**, 718–724 (2020).

48. J. S. Lee, S. Park, H. W. Jeong, J. Y. Ahn, S. J. Choi, H. Lee, B. Choi, S. K. Nam, M. Sa, J. S. Kwon, S. J. Jeong, H. K. Lee, S. H. Park, S.-H. Park, J. Y. Choi, S.-H. Kim, I. Jung, E.-C. Shin, Immunophenotyping of COVID-19 and influenza highlights the role of type I interferons in development of severe COVID-19. *Sci. Immunol.* **5**, eabd1554 (2020).

49. B. Israelow, E. Song, T. Mao, P. Lu, A. Meir, F. Liu, M. M. Alfajaro, J. Wei, H. Dong, R. J. Homer, A. Ring, C. B. Wilen, A. Iwasaki, Mouse model of SARS-CoV-2 reveals inflammatory role of type I interferon signaling. *J. Exp. Med.* **217**, e20201241 (2020).

50. J. Major, S. Crotta, M. Llorian, T. M. McCabe, H. H. Gad, S. L. Priestnall, R. Hartmann, A. Wack, Type I and III interferons disrupt lung epithelial repair during recovery from viral infection. *Science* **369**, 712–717 (2020).

51. F. Apel, L. Andreeva, L. S. Knackstedt, R. Streeck, C. K. Frese, C. Goosmann, K.-P. Hopfner, A. Zychlinsky, The cytosolic DNA sensor cGAS recognizes neutrophil extracellular traps. *Sci. Signal.* **14**, eaax7942 (2021).

52. J. Di Domizio, F. Gulen, F. Saidoune, V. V. Thacker, A. Yatim, K. Sharma, T. Nass, E. Guenova, M. Schaller, C. Conrad, C. Goepfert, L. De Leval, C. von Garnier, S. Berezowska, A. Dubois, M. Gilliet, A. Ablasser, The cGAS-STING pathway drives type I IFN immunopathology in COVID-19. *Nature* **603**, 145–151 (2022).

53. A. Y. Hsu, D. Wang, S. Liu, J. Lu, R. Syahirah, D. A. Bennin, J. Huttenlocher, D. M. Umulis, J. Wan, Q. Deng, Phenotypical microRNA screen reveals a noncanonical role of CDK2 in regulating neutrophil migration. *Proc. Natl. Acad. Sci. U.S.A.* **116**, 18561–18570 (2019).

54. A. F. Heiseke, B. H. Jeuk, A. Markota, T. Straub, H. A. Lehr, W. Reindl, A. B. Krug, IRAK1 drives intestinal inflammation by promoting the generation of effector Th cells with optimal Gut-homing capacity. *J. Immunol.* **195**, 5787–5794 (2015).

55. A. B. Dumbrepatil, S. Ghosh, K. A. Zegalia, P. A. Malec, J. D. Hoff, R. T. Kennedy, E. N. G. Marsh, Viperin interacts with the kinase IRAK1 and the E3 ubiquitin ligase TRAF6, coupling innate immune signaling to antiviral ribonucleotide synthesis. *J. Biol. Chem.* **294**, 6888–6898 (2019).

56. W. Sukhumavasi, C. E. Egan, E. Y. Denkers, Mouse neutrophils require JNK2 MAPK for Toxoplasma gondii-induced IL-12p40 and CCL2/MCP-1 release. *J. Immunol.* **179**, 3570–3577 (2007).

57. E. G. G. Sprenkeler, A. T. J. Tool, S. Henriet, R. van Bruggen, T. W. Kuijpers, Formation of neutrophil extracellular traps requires actin cytoskeleton rearrangements. *Blood* **139**, 3166–3180 (2022).

58. H. R. Thiam, S. L. Wong, R. Qiu, M. Kittisopikul, A. Vahabikashi, A. E. Goldman, R. D. Goldman, D. D. Wagner, C. M. Waterman, NETosis proceeds by cytoskeleton and endomembrane disassembly and PAD4-mediated chromatin decondensation and nuclear envelope rupture. *Proc. Natl. Acad. Sci. U.S.A.* **117**, 7326–7337 (2020).

59. J. W. Singer, A. Fleischman, S. Al-Fayoumi, J. O. Mascarenhas, Q. Yu, A. Agarwal, Inhibition of interleukin-1 receptor-associated kinase 1 (IRAK1) as a therapeutic strategy. *Oncotarget* **9**, 33416–33439 (2018).

60. A. E. Leitch, C. Haslett, A. G. Rossi, Cyclin-dependent kinase inhibitor drugs as potential novel anti-inflammatory and pro-resolution agents. *Br. J. Pharmacol.* **158**, 1004–1016 (2009).

61. Q. Wu, Q. Wu, V. Jacevic, T. C. C. Franca, X. Wang, K. Kuca, Selective inhibitors for JNK signalling: A potential targeted therapy in cancer. *J. Enzyme Inhib. Med. Chem.* **35**, 574–583 (2020).

62. J. M. Wild, J. C. Porter, P. L. Molyneaux, P. M. George, I. Stewart, R. J. Allen, R. Aul, J. K. Baillie, S. L. Barratt, P. Beirne, S. M. Bianchi, J. F. Blaikley, J. Brooke, N. Chaudhuri, G. Collier, E. K. Denneny, A. Docherty, L. Fabbri, M. A. Gibbons, F. V. Gleeson, B. Gooptu, I. P. Hall, N. A. Hanley, M. Heightman, T. E. Hillman, S. R. Johnson, M. G. Jones, F. Khan, R. Lawson, P. Mehta, J. A. Mitchell, M. Plate, K. Poinasamy, J. K. Quint, P. Rivera-Ortega, M. Semple, A. J. Simpson, D. Smith, M. Spears, L. G. Spencer, S. C. Stanel, D. R. Thickett, A. A. R. Thompson, S. L. Walsh, N. D. Weatherley, M. E. Weeks, D. G. Wootton, C. E. Brightling, R. C. Chambers, L. P. Ho, J. Jacob, K. P. Hanley, L. V. Wain, R. G. Jenkins, Understanding the burden of interstitial lung disease post-COVID-19: The UK Interstitial Lung Disease-Long COVID Study (UKILD-Long COVID). *BMJ Open Respir. Res.* **8**, (2021).

63. K. Imkamp, V. Bernal, M. Grzegorzcyk, P. Horvatovich, C. J. Vermeulen, I. H. Heijink, V. Guryev, H. A. M. Kerstjens, M. van den Berge, A. Faiz, Gene network approach reveals co-expression patterns in nasal and bronchial epithelium. *Sci. Rep.* **9**, 15835 (2019).

64. C. Huang, L. Huang, Y. Wang, X. Li, L. Ren, X. Gu, L. Kang, L. Guo, M. Liu, X. Zhou, J. Luo, Z. Huang, S. Tu, Y. Zhao, L. Chen, D. Xu, Y. Li, C. Li, L. Peng, Y. Li, W. Xie, D. Cui, L. Shang, G. Fan, J. Xu, G. Wang, Y. Wang, J. Zhong, C. Wang, J. Wang, D. Zhang, B. Cao, 6-month consequences of COVID-19 in patients discharged from hospital: A cohort study. *Lancet* **397**, 220–232 (2021).

65. L. C. Gandolfo, T. P. Speed, RLE plots: Visualizing unwanted variation in high dimensional data. *PLOS ONE* **13**, e0191629 (2018).

66. S. E. Khorsandi, A. D. Dokal, V. Rajeeve, D. J. Britton, M. S. Illingworth, N. Heaton, P. R. Cutillas, Computational analysis of cholangiocarcinoma phosphoproteomes identifies patient-specific drug targets. *Cancer Res.* **81**, 5765–5776 (2021).

67. D. N. Perkins, D. J. Pappin, D. M. Creasy, J. S. Cottrell, Probability-based protein identification by searching sequence databases using mass spectrometry data. *Electrophoresis* **20**, 3551–3567 (1999).

68. M. E. Ritchie, B. Phipson, D. Wu, Y. Hu, C. W. Law, W. Shi, G. K. Smyth, *limma* powers differential expression analyses for RNA-sequencing and microarray studies. *Nucleic Acids Res.* **43**, e47 (2015).

69. M. Hijazi, R. Smith, V. Rajeeve, C. Bessant, P. R. Cutillas, Reconstructing kinase network topologies from phosphoproteomics data reveals cancer-associated rewiring. *Nat. Biotechnol.* **38**, 493–502 (2020).

70. P. Casado, J. C. Rodriguez-Prados, S. C. Cosulich, S. Guichard, B. Vanhaesebroeck, S. Joel, P. R. Cutillas, Kinase-substrate enrichment analysis provides insights into the heterogeneity of signaling pathway activation in leukemia cells. *Sci. Signal.* **6**, rs6 (2013).

71. A. Manda-Handzlik, W. Bystrzycka, M. Wachowska, S. Sieczkowska, A. Stelmaszczyk-Emmel, U. Demkow, O. Ciepiela, The influence of agents differentiating HL-60 cells toward granulocyte-like cells on their ability to release neutrophil extracellular traps. *Immunol. Cell Biol.* **96**, 413–425 (2018).

72. A. Singanayagam, S. L. Loo, M. Calderazzo, L. J. Finney, M.-B. Trujillo Torralbo, E. Bakhsoliani, J. Girkin, P. Veerati, P. S. Pathinayake, K. S. Nichol, A. Reid, J. Footitt, P. A. B. Wark, C. L. Grainge, S. L. Johnston, N. W. Bartlett, P. Mallia, Antiviral immunity is impaired in COPD patients with frequent exacerbations. *Am. J. Physiol. Lung Cell. Mol. Physiol.* **317**, L893–L903 (2019).

73. E. Cavalier, J. Guiot, K. Lechner, A. Dutsch, M. Eccleston, M. Herzog, T. Bygott, A. Schomburg, T. Kelly, S. Holdenrieder, Circulating nucleosomes as potential markers to monitor COVID-19 disease progression. *Front. Mol. Biosci.* **8**, 600881 (2021).

A persistent neutrophil-associated immune signature characterizes post–COVID-19 pulmonary sequelae

Peter M. George, Anna Reed, Sujal R. Desai, Anand Devaraj, Tasnim Shahridan Faiez, Sarah Laverty, Amama Kanwal, Camille Esneau, Michael K.C. Liu, Faisal Kamal, William D.-C. Man, Sundeep Kaul, Suveer Singh, Georgia Lamb, Fatima K. Faizi, Michael Schuliga, Jane Read, Thomas Burgoyne, Andreia L. Pinto, Jake Micallef, Emilie Bauwens, Julie Candiracci, Mhammed Bougoussa, Marielle Herzog, Lavanya Raman, Blerina Ahmetaj-Shala, Stuart Turville, Anupriya Aggarwal, Hugo A. Farne, Alessia Dalla Pria, Andrew D. Aswani, Francesca Patella, Weronika E. Borek, Jane A. Mitchell, Nathan W. Bartlett, Arran Dokal, Xiao-Ning Xu, Peter Kelleher, Anand Shah, and Aran Singanayagam

Casting a wide NET on long COVID

A substantial number of individuals who recover from COVID-19 still present with long-term sequelae. Here, George *et al.* followed individuals after recovery from severe COVID-19 to identify features that distinguished those that had evidence of long-term pulmonary sequelae from those who made a full recovery. They found that a neutrophil-associated inflammatory phenotype was apparent in those who had persistent pulmonary symptoms, and evidence of neutrophil extracellular traps, or NETs, was found in the blood of these individuals. These data highlight a potential role for neutrophils in pulmonary long COVID.

View the article online
https://www.science.org/doi/10.1126/scitranslmed.abo5795
Permissions
https://www.science.org/help/reprints-and-permissions

Use of this article is subject to the Terms of service